Submillimeter wave spectroscopy and astronomical search for 1-propanimine

L. Margulès, A. Remijan, A. Belloche, R. A. Motiyenko, B. A. Mcguire, C. Xue, H. S. P. Müller, R. T. Garrod, K. M. Menten, J.-C. Guillemin

A&A 663, A132 (2022)
https://doi.org/10.1051/0004-6361/202243172

Astronomy & Astrophysics

Submillimeter wave spectroscopy and astronomical search for 1-propanimine⋆

L. Margulès[1], A. Remijan[2], A. Belloche[3], R. A. Motiyenko[1], B. A. McGuire[2,4], C. Xue[2,4], H. S. P. Müller[5], R. T. Garrod[6], K. M. Menten[3], and J.-C. Guillemin[7]

[1] Université de Lille, CNRS, UMR 8523, PhLAM, Physique des Lasers Atomes et Molécules, 59000 Lille, France
e-mail: laurent.margules@univ-lille.fr
[2] National Radio Astronomy Observatory, Charlottesville, VA 22903, USA
[3] Max-Planck-Institut für Radioastronomie, Auf dem Hügel 69, 53121 Bonn, Germany
[4] Department of Chemistry, Massachusetts Institute of Technology, Cambridge, MA 02139, USA
[5] Astrophysik/I. Physikalisches Institut, Universität zu Köln, Zülpicher Str. 77, 50937 Köln, Germany
[6] Departments of Chemistry and Astronomy, University of Virginia, Charlottesville, VA 22904, USA
[7] Univ Rennes, Ecole Nationale Supérieure de Chimie de Rennes, CNRS, ISCR UMR6226, 35000 Rennes, France

Received 21 January 2022 / Accepted 28 February 2022

ABSTRACT

Context. Methanimine, CH_2NH, and ethanimine, CH_3CHNH, were both detected in the interstellar medium (ISM), the former in the 1970s and the latter nearly a decade ago. By analogy with nitriles, for which hydrogen cyanide, acetonitrile, and ethyl cyanide are the most abundant, n-propanimine was suggested as a candidate for detection in the ISM.
Aims. To date, no measurements of the rotational spectrum of 1-propanimine have been made. We present measurements and an analysis of its spectrum in the millimeter- and submillimeter-wave domain in order to provide an accurate prediction that is required to search for this molecule in the ISM.
Methods. The rotational spectrum of propanimine was investigated from 150 to 470 GHz. Watson's asymmetric top Hamiltonian in the I^r representation and S reduction was used for the analysis. The new prediction allowed us to search for 1-propanimine toward the high-mass star forming region Sagittarius B2(N), the dark molecular cloud TMC-1, as well as a sample of low-mass protostellar objects. These sources were observed with the Atacama Large Millimeter/submillimeter Array, the Green Bank Telescope, or the IRAM 30 m telescope.
Results. A total of 585 and 296 transitions of the *E* and *Z*-1-propanimine, respectively, were newly assigned and fitted in the laboratory spectra recorded up to 470 GHz. Quantum numbers up to $J = 73$ and $K_a = 18$ were reached for the *E* isomer and $J = 56$ and $K_a = 17$ for the *Z* isomer. We report the nondetection of 1-propanimine toward all astronomical sources investigated in this work. We find in particular that 1-propanimine is at least 20 times less abundant than methanimine in the envelope of the high-mass star forming region Sagittarius B2(N).
Conclusions. The accurate spectroscopic prediction of its spectrum provided in this work will allow astronomers to continue the search for 1-propanimine in the ISM.

Key words. ISM: molecules – methods: laboratory: molecular – submillimeter: ISM – molecular data – astrochemistry – line: identification

1. Introduction

Carbon and nitrogen atoms can be connected together by a single, double, or triple bond. In the interstellar medium (ISM) more than 45 cyanides (including isocyanides) have been observed[1], but the number of detected compounds with a double or single bond between nitrogen and carbon atoms is much more limited. Six imines have been detected: methanimine, CH_2NH (Godfrey et al. 1973); *E*- and *Z*-ethanimine, CH_3CHNH (Loomis et al. 2013); *E*- and *Z*-cyanomethanimine, HNCHCN (Zaleski et al. 2013; Rivilla et al. 2019); and Z-2-propynimine, HCC-CHNH (Bizzocchi et al. 2020). Several compounds with a C = N double bond can be added: iminopropadienylidene HNCCC (Kawaguchi et al. 1992); ketenimine, also called ethenimine, CH_2CNH (Lovas et al. 2006); carbodiimide, HNCNH (McGuire et al. 2012); HCCN and CCN radicals (Guélin & Cernicharo 1991; Anderson & Ziurys 2014); the methylene amidogen H_2CN (Ohishi et al. 1994); and three isocyanates HNCO (Snyder & Buhl 1972), CH_3NCO (Cernicharo et al. 2016), and C_2H_5NCO (Rodríguez-Almeida et al. 2021).

It should be noted that imines, which have a permanent dipole moment of about 2D and often two stereoisomers (*E* and *Z*), are generally less easily detected by their rotational spectra than nitriles. The latter usually have a permanent dipole moment between 3 and 4D and have no stereoisomer issued from the CN bond due to its axial symmetry. How can imines form in the ISM? Several approaches have been considered mainly in the solid phase, but it should be noted that expecting a general behavior for imines in the ISM independently of the substituent is only a hypothesis. The reduction of nitriles to corresponding

⋆ Full Tables 2 and 3 are only available at the CDS via anonymous ftp to cdsarc.u-strasbg.fr (130.79.128.5) or via http://cdsarc.u-strasbg.fr/viz-bin/cat/J/A+A/663/A132
[1] http://www.astro.uni-koeln.de/cdms/molecules

imines on the surfaces of interstellar dust grains by atomic hydrogen bombardment has been proposed several times for methanimine (Godfrey et al. 1973), ethanimine (Loomis et al. 2013), or *Z*-cyanomethanimine (Rivilla et al. 2019). However, based on laboratory grain chemistry simulations, this approach appears unable to generate significant amounts of methanimine in the ISM (Theulé et al. 2011), and it seems to be even less efficient for substituted derivatives (Nguyen et al. 2019). Oxidation of amines to form imines by removal of dihydrogen could be accomplished by photolysis (Bossa et al. 2012), but amines like ethylamine or propargylamine corresponding to detected imines (ethanimine and propynimine, respectively) have not yet been detected or only tentatively in the case of ethylamine (Zeng et al. 2021), which makes this approach very hypothetical.

The reaction of ammonia on aldehydes followed by the elimination of one molecule of water could explain the formation of imines. The detection of α-aminoalcohols, which are intermediates in this type of reaction, could support this approach, but the rotational spectra of these kinetically unstable compounds have never been recorded. While thermal formation on matrix at 80 K has been demonstrated, their characterization in the gas phase has been limited to a detection in mass spectrometry during the warming of the solid in vacuo (Bossa et al. 2009). On the other hand, laboratory simulations of the formation of methanimine on interstellar grains by dehydration of the α-aminoalcohol intermediate did not allow the identification of the imine (Vinogradoff et al. 2012). Other approaches could be envisaged, such as using nitrogen radicals with various reagents (e.g., CO, H_2CO, CH_4) or ammonia with radicals, but to the best of our knowledge these approaches have never been rationalized in the aim to find a way for the synthesis of imines in the ISM. Recently, it has been proposed, on the basis of theoretical calculations, that methanimine could be the precursor of other imines (Lupi et al. 2020). It should be noted that all the imines detected in the ISM have corresponding nitriles that are abundant in certain astronomical environments (HCN for methanimine, CH_3CN for *E*- and *Z*-ethanimine, HC_3N for *Z*-propynimine, and NCCN for *E*- and *Z*-cyanomethanimine), even if the detection of NCCN, a compound without dipole moment, was made through the protonated derivative (Agúndez et al. 2015).

Consequently, ethyl cyanide (C_2H_5CN) being abundant in the ISM, we have identified 1-propanimine, C_2H_5CHNH (hereafter simply propanimine), which is the next complex compound after CH_2NH and CH_3CHNH, as a candidate for detection in the ISM. Since low boiling point imines in pure form can easily be synthesized by dehydrocyanation in vacuo of the corresponding α-aminonitrile (Guillemin & Denis 1988), we used this approach to record the millimeter wave spectrum of C_2H_5CHNH from 150 GHz to 470 GHz.

2. Experimental analysis

2.1. Synthesis

2-aminobutyronitrile ($C_2H_5CH(CN)NH_2$) was slowly vaporized in a reactor containing dry KOH in half-section and heated to 90 °C. A trap cooled at −80 °C removed high boiling point compounds and the gaseous flow of pure *E*- and *Z*-propanimine was condensed in a trap immersed in a liquid nitrogen bath (Guillemin & Denis 1988). As the propanimine was found to have a stability well below one minute in the cell, the synthesis had to take place during the measurements, and the gaseous flow of the imine was continuously introduced into the Pyrex cell of the spectrometer in slow flow mode.

2.2. Lille: Submillimeter wave spectra

The measurements in the frequency range under investigation (150–470 GHz) were performed using the Lille spectrometer (Zakharenko et al. 2015). The absorption cell was a Pyrex tube (6 cm diameter, 120 cm long). The sample pressure during measurements was about 10 Pa at room temperature; the line width was limited by Doppler broadening. The frequency ranges 150–330 and 400–470 GHz were covered with various active and passive frequency multipliers from VDI Inc. and an Agilent synthesizer (12.5–18.25 GHz) was used as the source of radiation. Estimated uncertainties for measured line frequencies are 50 kHz, which is a bit higher than our usual uncertainties (30 kHz). This is due to the fact that we had to use a frequency step two to three times larger than usual (from 60 kHz at 150 GHz up to 126 kHz at 470 GHz) in order to be faster because we had to work in a flow mode with a limited amount of samples.

3. Analysis of the laboratory spectra of propanimine

No spectroscopic studies of propanimine existed when we started this work. The first prediction of the spectra was done using spectroscopic parameters coming from density functional theory calculations at the B3LYP level of theory with a 6-311++g(3df, 2pd) basis set. The calculations were performed using the Gaussian 09 suite of programs (Frisch et al. 2009). As in the case of ethanimine, the *E* isomer was found to be more stable than the *Z* isomer (+3.16 kJ mol^{-1}, this energy difference includes the zero-point correction) (see Fig. 1). Considering the Boltzmann factor at room temperature, the lines of the *Z* isomer should be about four times less intense than the lines of the *E* isomer. However, the values of the dipole moment obtained from calculations are larger for the *Z* isomer (μ_a = 2.49 D, μ_b = 1.00 D) than those for the *E* isomer (μ_a = 1.12 D, μ_b = 0.75 D, μ_c = 1.57 D). Typically, in the centimeter and millimeter wave domain, the most intense transitions of complex organic molecules are the *R*-branch transitions related to the μ_a component of the dipole moment. The value of μ_a of the *Z* isomer is twice that of the *E* isomer because the intensity of a transition is proportional to μ^2, the spectra at room temperature for the two isomers will have similar intensities even if the *Z* isomer is 3.16 kJ mol^{-1} higher in energy than the *E* isomer, as illustrated in Fig. 2. In astronomical hot molecular cores with typical temperatures of 150–250 K both should be detectable.

The identification of the spectrum began with the transitions of the ^aR-branches. Even if there were large offsets with respect to the predictions made from the density functional theory calculations, the characteristic pattern of the branch was well reproduced, which allowed unambiguous identification. The offsets observed between the calculations and the experimental spectra at 160 GHz for the ^aR-branch band heads corresponding to J = 19–18 were +470 MHz and +290 MHz for the *Z* and *E* stereoisomers, respectively. All ^aR-branch lines were then analysed up to 470 GHz without difficulties. Then ^bR lines were searched for and included in the fit. Finally, nice *Q*-branch lines due to μ_c-type transitions could be observed for the *E* isomer above 400 GHz. It should be noted that these transitions do not exist for *Z* isomer because its μ_c is zero. Internal rotation splitting of the CH_3 group (for the *E* isomer) or hyperfine structure splitting caused by the ^{14}N nucleus are only resolvable in selected transitions at low frequencies. The two types of splitting were not resolved here.

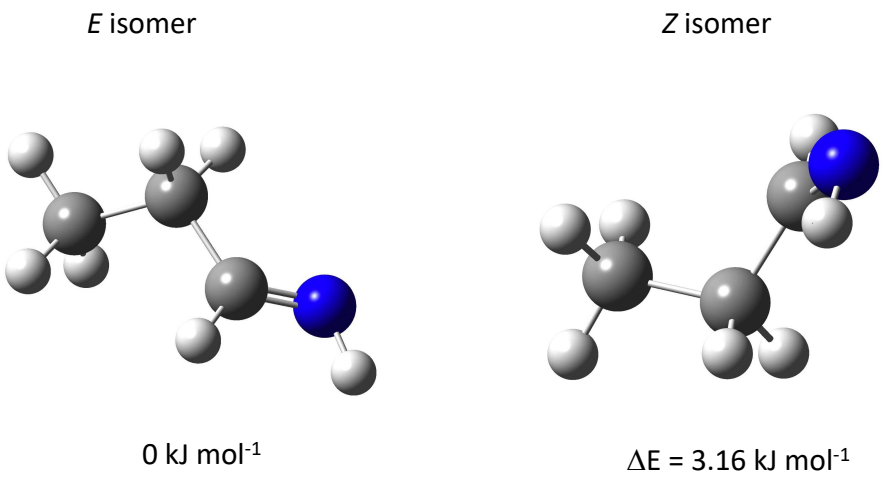

Fig. 1. *E* and *Z* stereoisomers of propanimine. Isomer *E*, which is more stable than isomer *Z*, was calculated to be 3.16 kJ mol^{-1} lower in energy (zero-point correction included) via the B3LYP/6-311++g(3df,2pd) procedure using the Gaussian 09 suite of programs (Frisch et al. 2009).

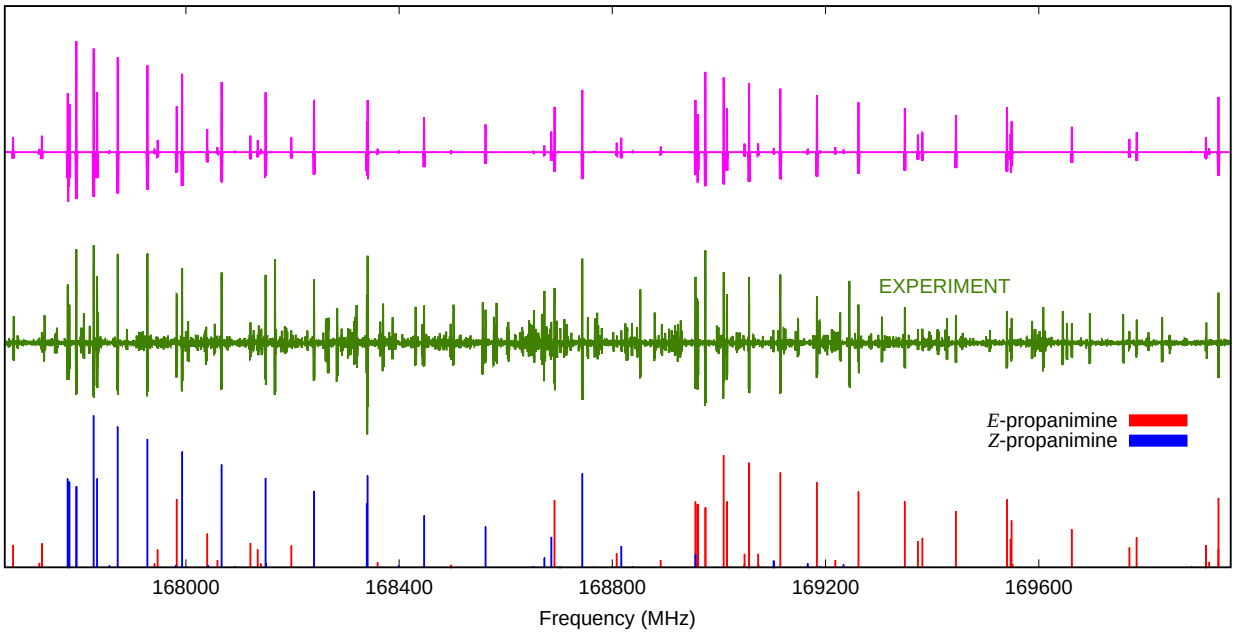

Fig. 2. Comparison of the experimental spectrum recorded at room temperature and the theoretical spectrum between 167.4 and 170.0 GHz. *Top*: simulated spectrum at 300 K for both isomers of propanimine. *Middle*: part of the experimental spectrum. *Bottom*: predictions for isomers *E* (in red) and *Z* (in blue).

A total of 585 distinct lines of the *E* isomer were assigned with maximum values for J and K_a of 73 and 18, respectively. Both A and S reductions were tested since this molecule is very close to the prolate limit with $\kappa = -0.9864$. The A reduction requires 24 parameters; using the S reduction with one additional parameter decreases the standard deviation of the fit from 146.1 to 39.4 kHz. Even with an additional parameter, the reduction S is more efficient in our case. A more detailed discussion on the advantage of the S reduction over the A reduction in the case of SO_2 with one and two ^{18}O can be found in Margulès et al. (2020b). The final fits and the prediction were done using this reduction for both stereoisomers. The spectra of the *Z* isomer looks different from that of the *E* isomer because of the lack of the μ_c dipole moment. The spectra of the *Z* isomer are less dense than those the *E* isomer. Finally, 296 distinct lines could be assigned for the *Z* conformer with maximum values for J and K_a of 56 and 17, respectively. The standard deviation of the fit is 48.4 kHz and 19 parameters were determined. We employed ASFIT (Kisiel 2001) for the fitting. The final set of parameters that we obtained are listed in Table 1. Part of the new measurements for the *E* and *Z* -propanimine are given in Tables 2 and 3, respectively. Owing to their large size, the complete versions of the global fit (full Tables 2 and 3) for the two stereoisomers are supplied at the CDS. The predicted spectra are available in standard .cat format (Pickett 1991) from the new database of the Lille spectroscopy group called the Lille Spectroscopic Database (`https://lsd.univ-lille.fr`). The predictions can be generated using various options (e.g., intensity units, temperature, and frequency range) that provide additional flexibility in the data access.

The tabulated values for the partition function are given in Table 4, with $Q_{tot}(T) = Q_{vib}(T) \times Q_{rot}(T)$. The rotational partition function was obtained directly at various temperatures from SPCAT (Pickett 1991). The vibrational contribution was

Table 1. Spectroscopic parameters of *E*- and *Z*-propanimine (in MHz) in the S reduction.

Parameter [a]	*E*-propanimine		*Z*-propanimine	
	This work	Theory [b]	This work	Theory [b]
A	24 185.2383 (13) [c]	24 524.014	23 925.25 (11)	24 200.587
B	4292.55416 (32)	4277.0318	4260.9794 (14)	4250.288
C	4156.59879 (32)	4147.1546	4129.2306 (13)	4124.526
$D_J \times 10^3$	4.87724 (26)	4.07194	4.70076 (38)	3.843750
$D_{JK} \times 10^3$	−106.5722 (25)	−91.291	−101.2483 (29)	−80.731
$D_K \times 10^3$	1097.331 (14)	988.674	981 (20)	884.409
$d_1 \times 10^3$	0.17719 (17)	0.142694	0.53846 (67)	0.399189
$d_2 \times 10^3$	0.083621 (39)	0.059202	0.02458 (31)	0.009272
$H_J \times 10^6$	0.05569 (10)		0.05279 (14)	
$H_{JK} \times 10^6$	−1.3048 (17)		−1.2524 (16)	
$H_{KJ} \times 10^6$	0.078 (14)		0.0 [d]	
$H_K \times 10^6$	63.376 (53)		0.0 [d]	
$h_1 \times 10^9$	18.300 (88)		5.12 (26)	
$h_2 \times 10^9$	−9.709 (35)		−10.40 (17)	
$h_3 \times 10^9$	0.2939 (62)		0.7708 (73)	
$L_J \times 10^{12}$	−0.857 (14)		−0.886 (18)	
$L_{JJK} \times 10^{12}$	30.21 (38)		28.55 (25)	
$L_{JK} \times 10^9$	−0.2809 (68)		−0.2938 (29)	
$L_{KKJ} \times 10^9$	−0.913 (23)		−1.746 (33)	
$L_K \times 10^9$	0.0 [d]		0.0 [d]	
$l_1 \times 10^{12}$	−0.768 (13)		−0.442 (34)	
$l_2 \times 10^{12}$	0.2239 (72)		0.491 (28)	
$l_3 \times 10^{12}$	0.0298 (23)		0.0 [d]	
$l_4 \times 10^{15}$	0.0 [d]		0.0 [d]	
$P_{JJK} \times 10^{15}$	−0.965 (33)		0.0 [d]	
$P_{JK} \times 10^{15}$	21.93 (95)		0.0 [d]	
$P_{KJ} \times 10^{15}$	−298.3 (77)		0.0 [d]	
$\lvert\mu_a\rvert, \lvert\mu_b\rvert, \lvert\mu_c\rvert$ [e]		1.12, 0.75, 1.57		2.49, 1.0, 0.0
Number of distinct lines	585		296	
Standard deviation of the fit	0.0394		0.0484	
Weighted deviation of fit	0.787		0. 967	

Notes. [a]Watson's S reduction has been used in the representation I^r. [b]Density functional theory calculations at the B3LYP level of theory with a 6-311++g(3df, 2pd) basis set. The calculations were performed using the Gaussian 09 suite of programs (Frisch et al. 2009). [c]Numbers in parentheses are one standard deviation in units of the least significant figures. [d]Fixed value. [e]Absolute dipole moment values in Debye.

calculated in the harmonic approximation (Gordy & Cook 1984), as we proceeded in our previous studies (see, e.g., Margulès et al. 2020c). Of the 27 vibrational modes, only the 7 with an energy level lower than 1000 cm^{-1} (1439 K) were considered. The other higher energy states have no influence on the calculation of the partition function. The harmonic frequencies of the vibrational modes used in the $Q_{\rm vib}(T)$ calculations were obtained from density functional theory calculations at the B3LYP level of theory with a 6-311++g(3df, 2pd) basis set.

4. Astronomical observations

4.1. Search for propanimine and related imines toward Sgr B2(N) with the GBT

As described in Remijan et al. (2022), the PRebiotic Interstellar Molecule Survey (PRIMOS)[2] was a key science program that started in 2008 January and concluded in 2011 July conducted with the Robert C. Byrd Green Bank Telescope (GBT) currently managed by the Green Bank Observatory (GBO). The PRIMOS project covers nearly all observable frequencies available to ground-based instrumentation from ~300 MHz to 48 GHz at high sensitivity (~3–9 mK rms) and spectral resolution (24.4 kHz). These observations were centered on the Sgr B2(N) Large Molecule Heimat (LMH) at $(\alpha, \delta)_{\rm J2000} = (17^{\rm h}47^{\rm m}19\overset{\rm s}{.}8, -28^\circ22'17\overset{''}{.}0)$.

Figure 3 shows the results of our attempt to detect the strongest transitions, including possible maser transitions, from C_2H_5CHNH between 8 and 43 GHz from the PRIMOS survey. Similar to the identification done in the laboratory spectra, we first searched for the more stable *E* -propanimine of C_2H_5CHNH. The calculated dipole moments of the *E* conformer (see Sect. 3) suggest that *c*-type transitions should be the strongest transitions and, as is typical for large asymmetric top molecules, *R*-branch transitions are also the strongest transitions observed except in

[2] Access to the entire PRIMOS data set, specifics of the observing strategy, and overall frequency coverage information is available at http://archive.nrao.edu by searching for GBT Program ID: AGBT07A_051.

Table 2. Measured frequencies of the *E*-propanimine and residuals from the fit.

Upper level			Lower level			Frequency(Unc.)	o.-c.
J''	K''_a	K''_c	J'	K'_a	K'_c	(in MHz)	(in MHz)
34	5	30	33	4	29	466 139.401(0.050)	–0.0509
34	5	29	33	4	29	466 149.401(0.050)	0.0322
34	5	30	33	4	30	466 374.636(0.050)	–0.0517
46	3	43	45	2	43	466 496.932(0.050)	0.0768
56	2	55	55	2	54	467 024.662(0.050)	–0.0644
20	8	12	19	7	12	467 256.923(0.050)	0.0012
20	8	12	19	7	13	467 256.923(0.050)	0.0012
20	8	13	19	7	12	467 256.923(0.050)	0.0012
20	8	13	19	7	13	467 256.923(0.050)	0.0012
56	1	55	55	1	54	467 456.647(0.050)	–0.0130
11	10	1	10	9	1	468 879.804(0.050)	–0.0164
11	10	1	10	9	2	468 879.804(0.050)	–0.0164
11	10	2	10	9	1	468 879.804(0.050)	–0.0164
11	10	2	10	9	2	468 879.804(0.050)	–0.0164
40	4	36	39	3	36	469 205.833(0.050)	–0.0581
56	3	54	55	3	53	469 632.984(0.050)	0.0050
39	4	36	38	3	36	469 805.004(0.050)	0.0271

Notes. The full fit is available at the CDS.

Table 3. Measured frequencies of the *Z*-propanimine and residuals from the fit.

Upper level			Lower level			Frequency(Unc.)	o.-c.
J''	K''_a	K''_c	J'	K'_a	K'_c	(in MHz)	(in MHz)
56	10	46	55	10	45	467 992.603(0.050)	–0.0301
56	10	47	55	10	46	467 992.603(0.050)	–0.0301
56	5	51	55	5	50	468 039.779(0.050)	0.0245
56	11	45	55	11	44	468 174.105(0.050)	–0.0649
56	11	46	55	11	45	468 174.105(0.050)	–0.0649
56	12	44	55	12	43	468 385.864(0.050)	–0.0466
56	12	45	55	12	44	468 385.864(0.050)	–0.0466
56	2	54	55	2	53	468 558.707(0.050)	0.0817
56	13	43	55	13	42	468 624.898(0.050)	–0.0127
56	13	44	55	13	43	468 624.898(0.050)	–0.0127
56	14	42	55	14	41	468 889.206(0.050)	–0.0062
56	14	43	55	14	42	468 889.206(0.050)	–0.0062
56	15	41	55	15	40	469177.452(0.050)	0.0064
56	15	42	55	15	41	469 233.007(0.050)	0.0631
56	16	40	55	16	39	469 488.589(0.050)	–0.0149
56	16	41	55	16	40	469 488.589(0.050)	–0.0149

Notes. The full fit is available at the CDS.

those cases where maser action greatly increases the line intensity, as seen with molecules such as HNCNH (McGuire et al. 2012), CH_3CONH_2 (Remijan et al. 2022), CH_3OCHO (Faure et al. 2014), and CH_2NH (Faure et al. 2018). For the *Z* isomer the situation is quite different as the calculated a-dipole moment, for example, is more than twice as large as the *E* isomer (see Sect. 3). As such, for the *Z* isomer, a-type transitions should typically be the strongest transitions observed. However, for completeness, we searched for all *R*- and *Q*-branch, *a*-, *b*-, and *c*-type transitions over the entire PRIMOS observing range for any emission or absorption features from either the *E* or *Z* -propanimine of C_2H_5CHNH. Unfortunately, no transitions of C_2H_5CHNH were detected above a 3σ detection limit at any frequency covered by the PRIMOS survey.

We used the software `MOLSIM` (Lee et al. 2021) to perform the single excitation temperature modeling and to estimate the upper limit for the spectra analysis of the PRIMOS survey. Synthetic spectra are produced with a single excitation temperature assumption that all transitions are thermalized and corrected for optical depth, as discussed in Turner (1991) and Mangum & Shirley (2015). In addition, we assumed a non-thermal background source of emission with a (beam-diluted) continuum antenna temperature $T_C[\mathrm{K}] = 10^{2.3} \times \nu[\mathrm{GHz}]^{-1.06}$ (Hollis et al. 2007). Assuming the continuum emission has a source size of ∼20″, the corresponding continuum brightness temperatures were obtained through dividing T_C by the beam dilution factor. We simulated the spectrum of C_2H_5CHNH assuming an excitation temperature of 5.8 K, a source size of ∼20″, and a line width (d*V*) of 10 km s^{-1}. However, as Fig. 3 illustrates, no C_2H_5CHNH transitions (in magenta and cyan for the *E* and *Z* isomers, respectively) were detected. To set an upper limit of C_2H_5CHNH, we used the RMS noise level from the C_2H_5CHNH pass bands from the transition with the strongest predicted intensity in a pass band with the lowest RMS noise level. A 3σ upper limit of 1.5×10^{13} cm^{-2} was found for the *E* isomer from the strongest predicted transition at 19 555.99 MHz (predicted line intensity of 7.9 mK in a pass band with an RMS noise of 2.6 mK) and 1.0×10^{13} cm^{-2} was found for the *Z* isomer from the strongest predicted transition at 8390.19 MHz (predicted line intensity of 7.6 mK in a pass band with 5 mK RMS).

It is now possible to compare the upper limit column density determined for C_2H_5CHNH to other detected imines toward the Sgr B2(N-LMH) region from earlier PRIMOS observations. Ketenimine (CH_2CNH) was first detected by Lovas et al. (2006). However, only three transitions were identified in that work, so a more complete analysis with additional transitions now detected from the PRIMOS survey is warranted. The measured dipole moments for CH_2CNH are $\mu_a = 0.434(1)$ D and $\mu_c = 1.371(6)$ D (Rodler et al. 1984). As such, *c*-type transitions will be more prominent; however, an investigation including all *P*-branch transitions ($\Delta J = -1$) and R-branch transitions ($\Delta J = 1$) from both *a*- and *c*-type transitions in the detectable range of the PRIMOS survey was done.

All the transitions detected in Lovas et al. (2006) were $\Delta J = -1$, *c*-type transitions. Fitting these transitions with `MOLSIM`, we find that the best fit to the 8(1,7)–9(0,9) and the 7(1,6)–8(0,8) transitions gives a total column density of CH_2CNH of $N_\mathrm{T} \sim 1.8 \times 10^{16}$ cm^{-2} assuming a source size of 20″, $\delta v = 10$ km s^{-1}, and $T_\mathrm{ex} = 5.8$ K. The fit (and all subsequent reported fits in this section) is the sum of all three velocity components at $v_\mathrm{LSR} = +64$, +73, and +82 km s^{-1} detected toward the Sgr B2(N-LMH) region in the PRIMOS survey. However, the 9(1,8)–10(0,10) transition at 4930.36 MHz contains material from a more extended area as the GBT beam at this frequency (153″) includes the Sgr B2(M) region. In this case, an additional contribution with a N_T of 1.75×10^{17} cm^{-2} from the Sgr B2(M) region at its nominal v_LSR is needed to accommodate the observed intensity. Furthermore, the 8(1,7)–9(0,9) transition shows contamination by an unidentified feature around 23173.42 MHz. In addition, the very low T_ex is necessary to account for the absorption feature seen at 41 524.29 MHz given the very low continuum emission of this region around 41 GHz (see Fig. 4).

The situation is not as clear for the *R*-branch, $\Delta J = 1$, *a*- and *c*-type transitions covered in the PRIMOS survey. In this case, because these transitions are detected mostly in emission,

Table 4. Rotational, vibrational, and total partition functions of *E*- and *Z*-propanimine at various temperatures.

	E-Propanimine			*Z*-Propanimine		
T (K)	$Q(T)_{rot}$	$Q(T)_{vib}$	$Q(T)_{tot}$	$Q(T)_{rot}$	$Q(T)_{vib}$	$Q(T)_{tot}$
300	42 349.806	5.980	253 245.391	42 855.317	6.044	259 007.986
225	27 551.665	3.404	93 776.339	27 884.838	3.432	95 699.098
150	14 977.978	1.955	29 275.249	15 160.670	1.964	29 772.002
75	5286.790	1.197	6328.685	5351.882	1.199	6414.655
37.5	1868.806	1.024	1913.176	1891.941	1.024	1937.409
18.75	661.513	1.001	661.863	669.721	1.001	670.084
9.375	234.625	1.000	234.625	237.536	1.000	237.536

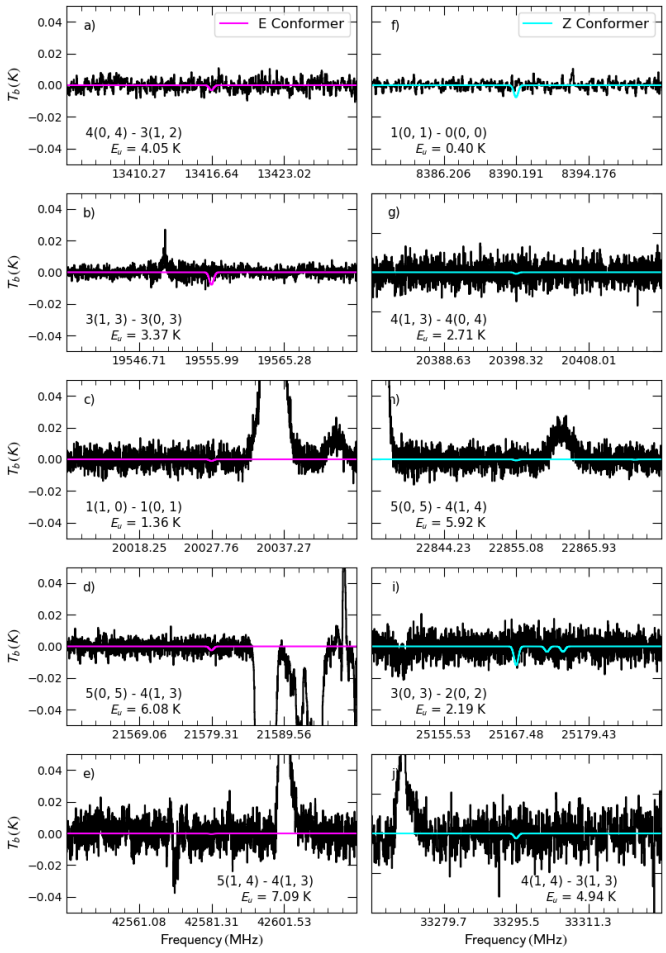

Fig. 3. Synthetic spectrum of C_2H_5CHNH. The *E* isomer transitions are presented in the first column in *panels a–e* (in magenta) and the *Z* isomer transitions are presented in the second column in *panels f–j* (in cyan). The spectrum was generated from the physical conditions and observing parameters described in Sect. 4.1 (i.e., T_{ex} = 5.8 K, source size of 20″, $N_T \sim 1.5 \times 10^{13}$ cm^{-2} for the *E* isomer and $N_T \sim 1.0 \times 10^{13}$ cm^{-2} for the *Z* isomer) overlaid on the GBT spectrum of Sgr B2(LMH) shown in black. Transition quantum numbers and upper state energy levels are at the bottom of each spectrum. No significant emission from C_2H_5CHNH transitions are detected beyond the 3σ upper limit. *Panels g* and *j* have an ordinate range between −0.1 and 0.1 K due to the noise level in the spectrum.

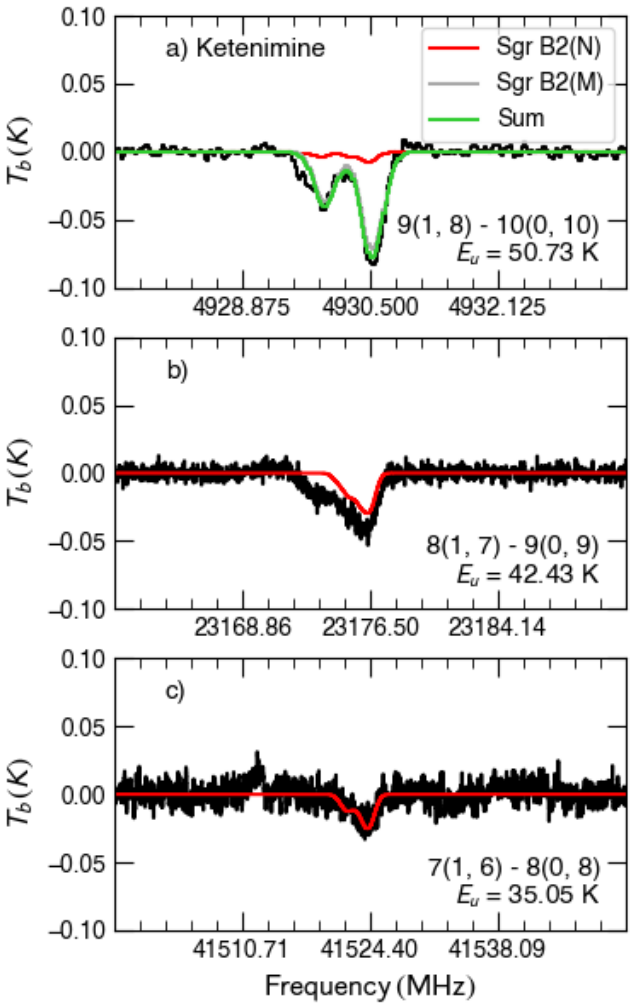

Fig. 4. Synthetic spectra of the P-branch ($\Delta J = -1$), c-type transitions of CH_2CNH overlaid on the GBT spectrum of Sgr B2. Transition quantum numbers are at the bottom of each spectrum. The synthetic spectra for the Sgr B2(N) components (red curve) were generated from the physical conditions and observing parameters described in Sect. 4.1 (i.e., T_{ex} = 5.8 K, source size = 20″, $N_T \sim 1.8 \times 10^{16}$ cm^{-2}). An additional contribution to the 4930 MHz absorption feature (gray curve) was modeled assuming the same T_{ex} and source size as that of Sgr B2(N), a v_{LSR} of +63 km s^{-1}, dV of 17 km s^{-1}, and N_T of $\sim 1.75 \times 10^{17}$ cm^{-2}. The sum of the synthetic absorption lines are shown by the green curve.

except in those cases where no feature is detected, it suggests that the emission is coming from a more compact and hot component of CH_2CNH, as was originally suggested by Lovas et al. (2006). Assuming the following physical properties, a derived total column density of CH_2CNH of $N_T \approx 4.6 \times 10^{16}$ cm^{-2}, a source size of 5″, a line width δv = 10 km s^{-1}, and an excitation temperature T_{ex} = 150 K for all three velocity components, can account for the measured intensity of the 12(0,12)–11(1,10) transition at 31 251.20 MHz and the nondetection of the 1(0, 1)–0(0, 0) and 2(0, 2)–1(0, 1) transitions at

19 133.25 MHz and 38 266.28 MHz, respectively. However, the 11(0,11)–10(1,9) transition at 13 212.59 MHz is still severely underpredicted, suggesting that this transition is either contaminated by an unknown feature or is somehow being pumped by maser action. In order to account for the measured intensity of this transition assuming a source size of 5″, $\delta v = 10$ km s^{-1}, and $T_{ex} = 150$ K, would require a total column density of CH_2CNH greater than $N_T \approx 2 \times 10^{18}$ cm^{-2}. Finally, the very weak (or non-existent) 13(0,13)–12(1,11) transition at 49184.07 MHz also cannot be explained by the parameters determined from the 31 251.20 MHz transition. The measured noise level at frequencies around 49 GHz is almost as high as the measured intensity of the lines at 31 and 13 GHz. In addition, 49 GHz is near the edge of the tuning range of the GBT Q-band receiver so the sensitivity and the aperture efficiency of the Q-band receiver fall off quite rapidly, thus making the detection of any feature at the extreme edge of the GBT tuning range problematic.

Nonetheless, from this analysis, using the derived total column density of CH_2CNH of $N_T \approx 1.8 \times 10^{16}$ cm^{-2} from the measured P-branch absorption features gives an upper limit to the column density ratio of C_2H_5CHNH/CH_2CNH of $<10^{-3}$. However, as can be seen from the descriptions above, this value is highly uncertain as only a very limited number of absorption features of CH_2CNH were detected, and one of them contains the absorption from an additional source: Sgr B2(M). A more thorough analysis, which is beyond the scope of this work, of the low-frequency detection of CH_2CNH is necessary to better constrain the column density and physical environments containing CH_2CNH.

Methanimine (CH_2NH) was first reported by Godfrey et al. (1973) toward Sgr B2(N). In a recent investigation by Faure et al. (2018), non-thermal excitation was investigated to try and determine the physical conditions leading to the measured intensities of the observed low-frequency maser emission features. A best fit was found for a H_2 density range between 6×10^2 and 6×10^6 cm^{-3} and an excitation temperature of $T_{ex} = 30$ K. From this fit the determined total column density of CH_2NH for the low-velocity cloud is $N_T = 2.5 \times 10^{14}$ cm^{-2} and for the high-velocity cloud is $N_T = 1 \times 10^{14}$ cm^{-2}. This gives an upper limit to the column density ratio of C_2H_5CHNH/CH_2NH of 0.04 (and a CH_2CNH/CH_2NH ratio of ∼57). Unfortunately, there is no accepted formation route that justifies the abundance of CH_2CNH being so much higher than CH_2NH, and further investigation of both species is warranted to further ascertain this apparent discrepancy.

Ethanimine (CH_3CHNH) was first reported by Loomis et al. (2013). The derived total column density of the E and Z stereoisomers of CH_3CHNH was determined to be $N_T \sim 2.3 \times 10^{13}$ cm^{-2} assuming that the source of CH_3CHNH fills the GBT beam and that $T_{ex} = 6$ K. Zaleski et al. (2013) also detected transitions of CH_3CHNH in both emission and absorption and speculated that, like other low-frequency transitions of other large molecules, these emission features could be due to maser activity. As such, the total derived CH_3CHNH column density determined from just the features detected in absorption was found to be $N_T \approx 7 \times 10^{13}$ cm^{-2} (over 20 transitions of CH_3CHNH were detected). This then gives a range of upper limits to the column density ratio of C_2H_5CHNH/CH_3CHNH between 0.7 and 0.2. Finally, E-cyanoethanimine (E-HNCHCN) was first reported by Zaleski et al. (2013) (nine transitions were detected all in absorption). By once again assuming that the source of E-HNCHCN fills the GBT beam and that $T_{ex} = 8$ K, a total column density of $N_T \approx 1,5 \times 10^{13}$ cm^{-2} was determined, nearly identical to the upper limit found for C_2H_5CHNH. It is likely that C_2H_5CHNH would be lower in abundance than these previously detected imines so the upper limit found for C_2H_5CHNH, which is actually comparable with the abundances of the other detected species, suggests that higher sensitivity observations reaching a lower noise limit is necessary for detecting this species in absorption as it does not appear that any transitions of C_2H_5CHNH are excited by maser action, which would otherwise ease in facilitating the detection.

4.2. Search for propanimine and related species toward Sgr B2(N1) with ALMA

4.2.1. ALMA observations

We used the imaging spectral line survey ReMoCA carried out toward the high-mass star forming protocluster Sgr B2(N) with the Atacama Large Millimeter/submillimeter Array (ALMA) during its cycle 4. The details of the observations and data reduction were reported in Belloche et al. (2019). The main features of the survey are summarized here. The phase center is located at the equatorial position $(\alpha, \delta)_{J2000} = (17^h47^m19\overset{s}{.}87, -28°22'16\overset{''}{.}0)$, which is halfway between the two hot molecular cores Sgr B2(N1) and Sgr B2(N2). The survey used five frequency tunings to cover the frequency range from 84.1 to 114.4 GHz at a spectral resolution of 488 kHz (1.7–1.3 km s^{-1}). The observations achieved a sensitivity per spectral channel that varies between 0.35 mJy beam^{-1} and 1.1 mJy beam^{-1} (rms), depending on the setup, with a median value of 0.8 mJy beam^{-1}. The angular resolution (HPBW) ranges from ∼0.3″ to ∼0.8″ with a median value of 0.6″ that corresponds to ∼4900 au at the distance of Sgr B2 (8.2 kpc, Reid et al. 2019). We used here an improved version of the data reduction, as described in Melosso et al. (2020a).

Following Belloche et al. (2019), we analyzed the spectrum obtained toward the position Sgr B2(N1S) at $(\alpha, \delta)_{J2000} = (17^h47^m19\overset{s}{.}870, -28°22'19\overset{''}{.}48)$. The advantage of this position, which is offset by about 1″ to the south of the main hot core Sgr B2(N1), is its lower continuum opacity compared to the peak of the hot core. To analyze the spectrum, we produced synthetic spectra under the assumption of local thermodynamic equilibrium (LTE) with the astronomical software Weeds (Maret et al. 2011). This assumption is justified by the high densities of the regions where hot-core emission is detected in Sgr B2(N) ($>1 \times 10^7$ cm^{-3}, see Bonfand et al. 2019). A best-fit synthetic spectrum was derived for each molecule separately, and then the contributions of all identified molecules were added together. Each species was modeled with a set of five parameters: size of the emitting region (θ_s), column density (N), temperature (T_{rot}), line width (ΔV), and velocity offset (V_{off}) with respect to the assumed systemic velocity of the source, $V_{sys} = 62$ km s^{-1}.

4.2.2. Nondetection of propanimine

In order to search for propanimine, C_2H_5CHNH, toward Sgr B2(N1S), we relied on the LTE parameters derived for methanimine, CH_2NH. The latter is clearly detected in its vibrational ground state (see Fig. B.1). We used the spectrocopic predictions of methanimine (tag 29518, version 2) available in the CDMS catalog (Müller et al. 2005), which are mainly based on the works of Krause & Sutter (1989), Dore et al. (2010, 2012), and Motoki et al. (2014). We selected the transitions of methanimine that are not too contaminated by emission or

Table 5. Rotational temperature of methanimine derived from its population diagram toward Sgr B2(N1S).

Molecule	States [(a)]	$T_{\rm fit}$ [(b)] (K)
CH_2NH	$v = 0$	220 (13)

Notes. [(a)]Vibrational states that were taken into account to fit the population diagram. [(b)]The standard deviation of the fit is given in parentheses. As explained in Sect. 3 of Belloche et al. (2016) and in Sect. 4.4 of Belloche et al. (2019), this uncertainty is purely statistical and should be viewed with caution. It may be underestimated.

absorption from other species to build a population diagram (Fig. B.2). Despite the small number of transitions, a broad range of upper-level energy is covered and a rotational temperature of 220 ± 13 K could be derived (Table 5). This temperature is consistent with the temperature of 223 ± 6 K that we derived from the ReMoCA survey for methylamine CH_3NH_2 (Kisiel et al. 2022). This suggests that both species trace the same layer of the hot core. Like in Kisiel et al. (2022) for methylamine, we adopted a temperature of 230 K to compute the LTE synthetic spectra of methanimine shown in red in Fig. B.1. The LTE parameters derived for methanimine are reported in Table 6 along with those previously obtained for methylamine.

Figure B.1 shows a discrepancy between the LTE synthetic spectrum of methanimine and the observed spectrum for the hyperfine multiplet $4_{0,4}$–$3_{1,3}$ at 105 794 MHz with an upper level energy, $E_{\rm up}/k$, of 31 K, while the hyperfine multiplet $8_{1,7}$–$7_{2,6}$ at 109892 MHz with $E_{\rm up}/k = 128$ K is well fitted. Given that extended emission in the former transition of methanimine was detected in Sgr B2 with the Mopra telescope (Jones et al. 2008) and that Halfen et al. (2013) obtained a low rotational temperature of 44 K for the emission of this molecule probed with the 10 m single-dish SubMillimeter Telescope and 12 m antenna of the Arizona Radio Observatory, we suspect that the transition detected with ALMA at this frequency is affected by spatial filtering of the cold extended component that may be somewhat optically thick and may partially mask the hot core emission at this frequency. This transition tends to bias the fit of the rotational temperature in Fig. B.2 toward lower values. This strengthens our choice of a slightly higher temperature of 230 K to model the spectrum of methanimine.

Assuming that the more complex molecule propanimine traces the same region as methanimine, we produced LTE synthetic spectra for the former species adopting the same parameters as for the latter with only the column density left as a free parameter. We employed the spectroscopic predictions derived for the *E* and *Z* stereoisomers of propanimine in Sect. 3. The LTE synthetic spectra of propanimine were used to search for emission of this molecule in the ReMoCA survey toward Sgr B2(N1S). Neither of its stereoisomers is detected, as illustrated in Figs. B.11 and B.12. The upper limits on their column densities, after accounting for the vibrational and conformational partition functions, are reported in Table 6.

To put the nondetection of propanimine toward Sgr B2(N1S) in a broader astrochemical context, we also report in Table 6 the column density upper limits that we obtained for four additional amines, ethylamine $C_2H_5NH_2$ (Fig. B.3), vinylamine $C_2H_3NH_2$ (Figs. B.4 and B.5), normal-propylamine $C_3H_7NH_2$ (Fig. B.6), and its branched isomer iso-propylamine (Fig. B.7), as well as two other imines, ethanimine CH_3CHNH (Figs. B.8 and B.9) and ketenimine CH_2CNH (Fig. B.10). References of the spectroscopic works used to compute the LTE synthetic spectra of these species are given in Appendix B.

Table 6 indicates that propanimine is at least six times less abundant than methanimine in Sgr B2(N1S). The *E* and *Z* isomers of ethanimine, which has a degree of molecular complexity between these two molecules, are found to be at least six and ten times less abundant than methanimine, respectively. As it is unlikely that propanimine and ethanimine have similar column densities, this suggests that the upper limit derived for propanimine is far from its true column density, maybe by as much as one order of magnitude. We note that the synthetic spectra of ethanimine shown in Figs. B.8 and B.9 may suggest the presence of this molecule in Sgr B2(N1S), but there are too few unblended transitions to claim a detection, even a tentative one. Loomis et al. (2013) detected ethanimine toward Sgr B2(N) on larger scales with a low excitation temperature of ~6 K (albeit with a complex mixture of lines in emission and absorption) in the frame of the PRIMOS survey[2] with the GBT (see Sect. 4.1). The spectral confusion at the scales probed with the ReMoCA survey prevents us from detecting in a robust way the presence of ethanimine on smaller scales in the hot core.

Ethylamine $C_2H_5NH_2$ and methylamine CH_3NH_2 share the same structural difference as ethanamine CH_3CHNH and methanimine CH_2NH (a CH_2 group). Interestingly, we find similar lower limits for the abundance ratios $CH_3NH_2/C_2H_5NH_2$ and CH_2NH/CH_3CHNH (5.4 and 5.8, respectively, if we take the *E* isomer of ethanimine as more representative). In contrast, the lower limits we obtain for the next stage in complexity is much more constraining for the imines ($CH_2NH/C_2H_5CHNH > 6$) than for the amines ($CH_3NH_2/C_3H_7NH_2 > 1$ for both the straight and branched forms of propylamine). Finally, we find that vinylamine $C_2H_3NH_2$ is at least eight times less abundant than methylamine and ketenimine CH_2CNH is at least 19 times less abundant than methanimine. We note, however, that the transition frequencies of vinylamine between the tunneling states are uncertain, with calculated uncertainties on the order of 3 MHz for the transitions shown in Fig. B.5; the true uncertainties could be even larger. Therefore, it could be useful to revisit the rotational spectrum of vinylamine, in particular the rotation-tunneling transitions between the states 0^+ and 0^-.

The lower limits to the ratios $CH_3NH_2/C_2H_5NH_2$ and $CH_3NH_2/C_2H_3NH_2$ obtained toward Sgr B2(N1S) (5.4 and 8, respectively) can be compared to the ratios obtained by Zeng et al. (2018, 2021) toward the nearby shocked region G+0.693–0.027 (12 and 7, respectively, the former being only tentative). If their COM chemical composition is similar, despite the different physical processes that desorb the molecules from the grain surfaces in these two regions (thermal heating versus turbulent shocks), then we may be very close to a detection of vinylamine in Sgr B2(N1S), while the upper limit to the column density of ethylamine would still be at least twice as high as its actual column density. Finally, Zeng et al. (2018) derived a column density ratio CH_2NH/CH_3NH_2 of 0.2, which is a factor three lower than the ratio we obtained for Sgr B1(N1S), suggesting differences in the chemistries of these two regions.

4.3. Searches in GOTHAM and ASAI Data

We also conducted searches toward the nine sources shown in Table 7 using data from the GOTHAM Project (GBT Observations of TMC-1: Hunting Aromatic Molecules) and the publicly available Astrochemical Surveys at IRAM (ASAI) Large Program data. The GOTHAM observations (McGuire et al. 2020)

Table 6. Parameters of our best-fit LTE model of methylamine and methanimine toward Sgr B2(N1S), and upper limits for ethylamine, vinylamine, normal- and iso-propylamine, ethanimine, ketenimine, and propanimine.

Molecule	Status [a]	N_{det} [b]	θ_s [c] ($''$)	T_{rot} [d] (K)	N [e] (cm^{-2})	F_{vib} [f]	F_{conf} [g]	ΔV [h] (km s^{-1})	V_{off} [i] (km s^{-1})	$\frac{N_{ref}}{N}$ [j]
Methylamine										
CH_3NH_2 [k](⋆)	d	15	2.0	230	1.4 (18)	1.25	–	5.0	0.0	1
Ethylamine										
anti-$C_2H_5NH_2$	n	0	2.0	230	<2.5 (17)	1.74	2.43	5.0	0.0	>5.4
Vinylamine										
$C_2H_3NH_2$ within 0^- and 0^+	n	0	2.0	230	<1.7 (17)	1.27	–	5.0	0.0	>8.3
$C_2H_3NH_2$ between 0^- and 0^+	n	0	2.0	230	<1.8 (17)	1.27	–	5.0	0.0	>7.7
n-Propylamine										
Trans-trans-n-$C_3H_7NH_2$	n	0	2.0	230	<1.3 (18)	3.71	5.64	5.0	0.0	>1.1
iso-Propylamine										
trans-i-$C_3H_7NH_2$	n	0	2.0	230	<1.4 (18)	2.55	1.78	5.0	0.0	>1.0
Methanimine										
CH_2NH(⋆)	d	4	2.0	230	9.0 (17)	1.00	–	5.0	0.0	1
Ethanimine										
E-CH_3CHNH	n	0	2.0	230	<1.6 (17)	1.55	–	5.0	0.0	>5.8
Z-CH_3CHNH	n	0	2.0	230	<9.5 (16)	1.58	–	5.0	0.0	>9.5
Ketenimine										
CH_2CNH	n	0	2.0	230	<4.7 (16)	1.17	–	5.0	0.0	>19
Propanimine										
E-C_2H_5CHNH	n	0	2.0	230	<1.5 (17)	3.54	1.19	5.0	0.0	>6.1
Z-C_2H_5CHNH	n	0	2.0	230	<2.0 (17)	3.58	6.22	5.0	0.0	>4.5

Notes. [a]d: detection, n: nondetection. [b]Number of detected lines (conservative estimate, see Sect. 3 of Belloche et al. 2016). One line of a given species may mean a group of transitions of that species that are blended together. [c]Source diameter (FWHM). [d]Rotational temperature. [e]Total column density of the molecule. x (y) means $x \times 10^y$. For vinylamine, the two sets of transitions belong to the same species, and each column density corresponds to the total column density of the molecule. For propanimine the two stereoisomers were modeled as independent species, and a isomer correction (F_{iso}) was applied a posteriori, such that each column density corresponds to the total column density of propanimine. For ethanimine the two isomers were modeled as independent species because of their large barrier to isomerization, and each column density corresponds to the column density of the respective isomer. [f]Correction factor that was applied to the column density to account for the contribution of vibrationally excited states in the cases where this contribution was not included in the partition function of the spectroscopic predictions. [g]Correction factor that was applied to the column density to account for the contribution of other isomer in the cases where this contribution could be estimated but was not included in the partition function of the spectroscopic predictions. [h]Line width (FWHM). [i]Velocity offset with respect to the assumed systemic velocity of Sgr B2(N1S), $V_{sys} = 62$ km s^{-1}. [j]Column density ratio, with N_{ref} the column density of the previous reference species flagged with a star (⋆). [k]The parameters were derived from the ReMoCA survey by Kisiel et al. (2022).

Table 7. Source parameters assumed and resulting upper limits for *E*-propanimine, *Z*-propanimine, and methanimine in each set of observations.

Source	Telescope	$\theta_s^{(\dagger)}$ ($''$)	T_{bg} (K)	ΔV (km s^{-1})	T_{ex} (K)	*E*-C_2H_5CHNH N_T (cm^{-2})(‡)	*Z*-C_2H_5CHNH N_T (cm^{-2})(‡)	CH_2NH N_T (cm^{-2})(‡)	Refs.
Barnard 1	IRAM	–	2.7	0.8	10	<2 (12)	<8 (11)	<5 (11)	1, 2
IRAS 4A	IRAM	–	2.7	1.3	16.7	<1 (13)	<3 (12)	9 (11)	1, 3, (∗)
L1157B1	IRAM	–	2.7	8	60	<1 (13)	<4 (12)	<2 (12)	4
L1157mm	IRAM	–	2.7	3	60	<8 (12)	<3 (12)	<1 (12)	4
L1448R2	IRAM	–	2.7	8	60	<3 (13)	<1 (13)	<4 (12)	5
L1527	IRAM	–	2.7	0.5	12	<1 (12)	<4 (11)	<3 (11)	5, 6
L1544	IRAM	–	2.7	0.5	10	<1 (12)	<3 (11)	<2 (12)	7, 8
SVS13A	IRAM	0.3	2.7	3	80	<2 (16)	<2 (16)	<3 (15)	1, 3
TMC1	GBT, IRAM	–	2.7	0.3	7	<9 (11)	<3 (11)	<1 (12)	9, 10

Notes. [†]Except where noted, the source is assumed to fill the beam. [‡]3σ upper limit to the column density, expressed as in Table 6 where $x(y)$ means $x \times 10^y$. [∗]Values for ΔV and T_{ex} for *E*- and *Z*-propanimine were set to those determined for methanimine (see text).
References: [1] Melosso et al. (2018); [2] Cernicharo et al. (2018); [3] Higuchi et al. (2018); [4] McGuire et al. (2015); [5]Jørgensen et al. (2002); [6] Araki et al. (2017); [7] Hily-Blant et al. (2018); [8] Crapsi et al. (2005); [9] McGuire et al. (2018); [10] Gratier et al. (2016).

target the cyanopolyyne peak of the TMC-1 dark molecular cloud using the 100 m Robert C. Byrd Green Bank Telescope (GBT) and cover roughly 8–11.6 GHz and 18–29.5 GHz, with a few small gaps; the data used are from the DR2 reduction detailed in McGuire et al. (2021). The ASAI spectra cover spectra in the 2–3 mm wavelength region and include a range of source types from cold dark clouds (including TMC-1) to Class 0/1 protostars and shocked outflows, with observational details available in Lefloch et al. (2018).

4.3.1. *E*- and *Z*-propanimine

Searches for the *E* and *Z* stereoisomers of propanimine resulted in nondetections in all sources. We derived upper limits to the column density in each source using the `MOLSIM` software package (Lee et al. 2021) and the formalisms outlined in Turner (1991), which assume that the molecules are well described by a single excitation temperature and include corrections for optical depth. For each source, because these are nondetections, we had to make assumptions about the physical conditions used to derive the upper limits. The set of parameters given in Table 7 was chosen to be representative of typical molecular detections within each source (references given in the final column), and are those we commonly used for this data set in the past (see, e.g., Margulès et al. 2020a). In the case of NGC 1333 IRAS 4A (hereafter IRAS 4A), the values for the line width (ΔV) and excitation temperature ($T_{\rm ex}$) were set to those determined for methanimine (see below).

4.3.2. Methanimine

We also searched all of these sources for CH_2NH, and found a solid detection in only one: IRAS 4A. Three lines, the $2_{0,2}-1_{0,1}$, $4_{0,4}-3_{0,3}$, and $4_{1,3}-3_{1,2}$ at 127857, 254685, and 266270 MHz, respectively, were seen above the noise level. A rotation diagram (Fig. 5) for these lines results in derived values of $T_{\rm ex} = 16.7^{+8.5}_{-5.1}$ K and $N_{\rm T} = 9^{+9}_{-4} \times 10^{11}$ cm^{-2}. The observed emission features from the ASAI data, as well as a simulation of the CH_2NH emission using the derived parameters, is shown in Fig. 6. The simulations agree with the observations within $\sim 3\sigma$. It is also possible that the source does not completely fill the beam, and thus some of the disagreement may be due to the substantially larger beam at 128 GHz versus near 260 GHz. For all other sources, 3σ upper limits are provided alongside those for *E*- and *Z*-propanimine in Table 7. We note that in the spectra for both L1157B1 and L1157mm there are features suggestive of methanimine emission just below the 3σ noise level for several of the brightest transitions, suggesting a deeper integration would likely result in a robust detection.

5. Discussion

We studied the rotational spectra of both stereoisomers (*E* and *Z*) of propanimine (C_2H_5CHNH). We analyzed some transitions with different selection rules up to high quantum numbers. The line catalog obtained from this analysis is very accurate up to at least 600 GHz. Only the ground vibrational state was investigated here. Because both isomers exhibit one low-lying vibrational mode below 100 cm^{-1} (143 K), these vibrational states should certainly be studied in the future if there is a detection of propanimine in the ISM.

We are currently working on analyzing the rotational spectra of ethanimine (CH_3CHNH). Previous studies of this molecule (Lovas et al. 1980; Loomis et al. 2013; Melli et al. 2018) did not provide a secure prediction in the same range as propanimine up to 600 GHz. An accurate catalog could be generated only up to 150 GHz, and was limited to low K_a values (0 and 1) up to 300 GHz. We recorded the spectra up to 650 GHz; the analysis is in progress. Unlike for propanimine, the internal rotation of the methyl group of ethanimine must be treated because it produces observable splittings. In addition to this, the hyperfine structure is also observable. Finally, there is a Coriolis interaction between torsionally and vibrationally excited states. V.V. Ilyushin (Institut of Radio Astronomy, Kharkiv, Ukraine) is currently developing the code in order to handle this interaction.

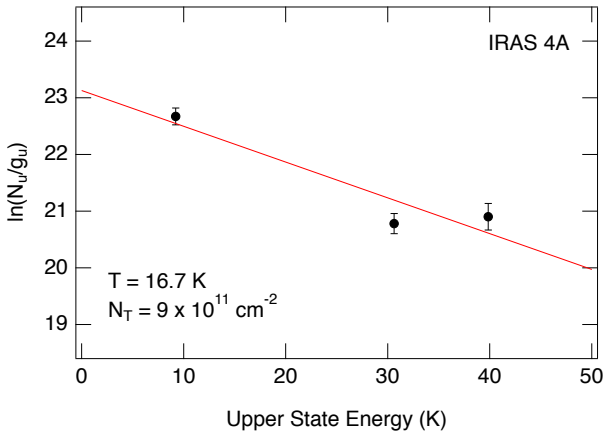

Fig. 5. Rotation diagram for CH_2NH in the ASAI data toward IRAS 4A. The error bars are derived from the statistical uncertainties in the Gaussian fits to the line shape of the emission features for each transition.

Our search for propanimine in several interstellar sources using various radio and millimeter wavelength astronomical surveys was unfortunately not successful. Propanimine is not detected in Sgr B2(N1), the main hot core of Sgr B2(N), with ALMA (Sect. 4.2) or on larger scales around this hot core with the GBT (Sect. 4.1). The GBT upper limit to the abundance ratio of propanimine to methanimine on large scales around Sgr B2(N) is 0.04, four times more constraining than the upper limit obtained for the hot core with ALMA (0.17). This upper limit is comparable to the upper limit obtained with ALMA for the abundance ratio of ethanimine to methanimine (0.18, see Sect. 4.2). Ethanimine was detected with the GBT with an abundance of 0.07–0.2 with respect to methanimine (Sect. 4.1), a range that brackets the ALMA upper limit, and we actually reported in Sect. 4.2 hints of the presence of ethanimine in the ALMA spectra. Taken together, this suggests that ethanimine may well be present in the hot core at a similar level, with respect to methanimine, to that in the surrounding envelope. This could suggest that the formation of both imines occurs early on in the star formation process.

This similarity in the imine chemistry of the two environments may also suggest that the ALMA upper limit for propanimine toward Sgr B2(N1) is more than a factor of four away from a detection. Given that the ReMoCA survey has nearly reached the spectral confusion limit on this hot core, there is little hope that propanimine can be detected in the future at 3 mm toward this source, unless even higher angular resolution observations manage to probe smaller regions with even narrower line widths. In addition, as stated in Sect. 4.1, given the scarcity of spectral features at centimeter wavelengths, and the overall sensitivity achievable at those wavelengths, it may be possible to detect

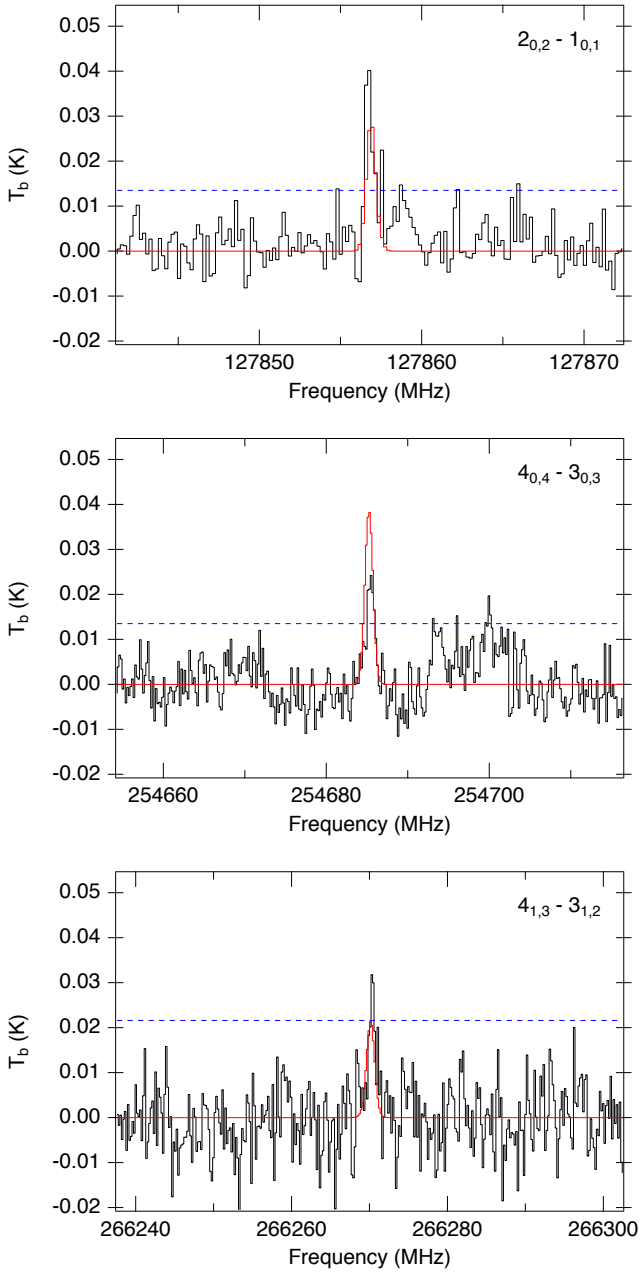

Fig. 6. Detected lines of CH_2NH toward IRAS 4A. The ASAI spectra are shown in black, while a single-excitation temperature simulation of the CH_2NH emission using the derived parameters is overlaid in red. Each panel is ~70 km s^{-1} in width. The 3σ local noise level is shown as a dashed blue line in each panel.

propanimine in absorption with longer integration times on the GBT.

For the ASAI and GOTHAM samples of sources, most upper limits derived for the *E* -propanimine are higher than or similar to the upper limits obtained for methanimine. Given that we expect a priori propanimine to be much less abundant than methanimine, this indicates that much more sensitive observations would be required to continue the search for both imines toward these sources. For the only source with a methanimine detection, IRAS 4A, the upper limit obtained for propanimine is more than one order of magnitude higher than the column density of methanimine, which means that an improvement by much more than one order of magnitude in sensitivity would be required to continue the search for propanimine.

6. Conclusion

Millimeter and submillimeter wave spectra of the *E* and *Z* stereoisomers of propanimine were assigned up to 470 GHz. This has permitted us to produce accurate predictions of the spectra of both isomers and made possible a search for this molecule in the ISM. Unfortunately, only nondetections could be reported in this work toward a sample of star forming regions targeted with various radio astronomical surveys. The most stringent constraint was obtained for the envelope of Sgr B2(N) where propanimine is at least 20 times less abundant than methanimine. The spectroscopic predictions are now available to the astrophysical community, enabling future searches for propanimine as more sensitive surveys become available.

Acknowledgements. This work was supported by the Programme National "Physique et Chimie du Milieu Interstellaire" (PCMI) of CNRS/INSU with INC/INP co-funded by CEA and CNES. J.C.G. thanks the Centre National d'Etudes Spatiales (CNES) for a grant. This paper makes use of the following ALMA data: ADS/JAO.ALMA#2016.1.00074.S. ALMA is a partnership of ESO (representing its member states), NSF (USA), and NINS (Japan), together with NRC (Canada), NSC and ASIAA (Taiwan), and KASI (Republic of Korea), in cooperation with the Republic of Chile. The Joint ALMA Observatory is operated by ESO, AUI/NRAO, and NAOJ. The interferometric data are available in the ALMA archive at https://almascience.eso.org/aq/. Part of this work has been carried out within the Collaborative Research Centre 956, subproject B3, funded by the Deutsche Forschungsgemeinschaft (DFG) – project ID 184018867. A.B. thanks M. Melosso for providing spectroscopic predictions of propylamine and ethanimine in electronic format. RTG acknowledges support from the National Science Foundation (grant No. AST 19-06489).

References

Agúndez, M., Cernicharo, J., De Vicente, P., et al. 2015, A&A, 579, L10
Anderson, J., & Ziurys, L. M. 2014, ApJ, 795, L1
Apponi, A. J., Sun, M., Halfen, D. T., Ziurys, L. M., & Müller, H. S. P. 2008, ApJ, 673, 1240
Araki, M., Takano, S., Sakai, N., et al. 2017, ApJ, 847, 0
Belloche, A., Müller, H. S. P., Garrod, R. T., & Menten, K. M. 2016, A&A, 587, A91
Belloche, A., Garrod, R. T., Müller, H. S. P., et al. 2019, A&A, 628, A10
Bizzocchi, L., Prudenzano, D., Rivilla, V. M., et al. 2020, A&A, 640, A98
Bonfand, M., Belloche, A., Garrod, R. T., et al. 2019, A&A, 628, A27
Bossa, J., Theule, P., Duvernay, F., & Chiavassa, T. 2009, ApJ, 707, 1524
Bossa, J.-B., Borget, F., Duvernay, F., et al. 2012, Australian J. Chem., 65, 129
Brown, R. D., Godfrey, P. D., Kleibomer, B., Pierlot, A. P., & McNaughton, D. 1990, J. Mol. Spectr., 142, 195
Cernicharo, J., Kisiel, Z., Tercero, B., et al. 2016, A&A, 587, L4
Cernicharo, J., Lefloch, B., Agúndez, M., et al. 2018, ApJ, 853, L22
Crapsi, A., Caselli, P., Walmsley, C. M., et al. 2005, ApJ, 619, 379
Degli Esposti, C., Dore, L., & Bizzocchi, L. 2014, A&A, 565, A66
Dore, L., Bizzocchi, L., Degli Esposti, C., & Gauss, J. 2010, J. Mol. Spectr., 263, 44
Dore, L., Bizzocchi, L., & Degli Esposti, C. 2012, A&A, 544, A19
Faure, A., Remijan, A. J., Szalewicz, K., & Wiesenfeld, L. 2014, ApJ, 783, 72
Faure, A., Lique, F., & Remijan, A. J. 2018, J. Phys. Chem. Lett., 9, 3199
Fischer, E., & Botskor, I. 1982, J. Mol. Spectr., 91, 116
Frisch, M., Trucks, G., Schlegel, H. B., et al. 2009, Gaussian, Inc., Wallingford, CT, 200
Godfrey, P., Brown, R., Robinson, B., & Sinclair, M. 1973, ApJ, 13, 119
Gordy, W., & Cook, R. L. 1984, Microwave Molecular Spectra, 3rd edn. (New York: Wiley)
Gratier, P., Majumdar, L., Ohishi, M., et al. 2016, ApJS, 225, 25
Guélin, M., & Cernicharo, J. 1991, A&A, 244, L21
Guillemin, J.-C., & Denis, J.-M. 1988, Tetrahedron, 44, 4431
Halfen, D. T., Ilyushin, V. V., & Ziurys, L. M. 2013, ApJ, 767, 66
Higuchi, A. E., Sakai, N., Watanabe, Y., et al. 2018, ApJ, 236, 0
Hily-Blant, P., Faure, A., Vastel, C., et al. 2018, MNRAS, 480, 1174
Hollis, J. M., Jewell, P. R., Remijan, A. J., & Lovas, F. J. 2007, ApJ, 660, L125
Jones, P. A., Burton, M. G., Cunningham, M. R., et al. 2008, MNRAS, 386, 117

Jørgensen, J. K., Schöier, F. L., & van Dishoeck, E. F. 2002, A&A, 389, 908
Kawaguchi, K., Takano, S., Ohishi, M., et al. 1992, ApJ, 396, L49
Kisiel, Z. 2001, in Spectroscopy from Space (Berlin: Springer), 91
Kisiel, Z., Kolesniková, L., Belloche, A., et al. 2022, A&A, 657, A99
Krause, H., & Sutter, D. H. 1989, Zeitschrift Naturforschung Teil A, 44, 1063
Lee, K. L. K., Loomis, R. A., Xue, C., El-Abd, S., & McGuire, B. A. 2021, https://doi.org/10.5281/zenodo.5497790
Lefloch, B., Bachiller, R., Ceccarelli, C., et al. 2018, MNRAS, 477, 4792
Loomis, R. A., Zaleski, D. P., Steber, A. L., et al. 2013, ApJ, 765, L9
Lovas, F. J., Suenram, R. D., Johnson, D. R., Clark, F. O., & Tiemann, E. 1980, J. Chem. Phys., 72, 4964
Lovas, F. J., Hollis, J. M., Remijan, A. J., & Jewell, P. R. 2006, ApJ, 645, L137
Lupi, J., Puzzarini, C., & Barone, V. 2020, ApJ, 903, L35
Mangum, J. G., & Shirley, Y. L. 2015, PASP, 127, 266
Maret, S., Hily-Blant, P., Pety, J., Bardeau, S., & Reynier, E. 2011, A&A, 526, A47
Margulès, L., Ilyushin, V., McGuire, B. A., et al. 2020a, J. Mol. Spectr., 371, 111304
Margulès, L., Motiyenko, R. A., & Demaison, J. 2020b, J. Quant. Spectr. Rad. Transf., 253, 107153
Margulès, L., McGuire, B. A., Evans, C. J., et al. 2020c, A&A, 642, A206
McGuire, B. A., Loomis, R. A., Charness, C. M., et al. 2012, ApJ, 758, L33
McGuire, B. A., Carroll, P. B., Dollhopf, N. M., et al. 2015, ApJ, 812, 1
McGuire, B. A., Burkhardt, A. M., Kalenskii, S. V., et al. 2018, Science, 359, 202
McGuire, B. A., Burkhardt, A. M., Loomis, R. A., et al. 2020, ApJ, 900, L10
McGuire, B. A., Loomis, R. A., Burkhardt, A. M., et al. 2021, Science, 371, 1265
Mcnaughton, D., & Robertson, E. G. 1994, J. Mol. Spectr., 163, 80
Melli, A., Melosso, M., Tasinato, N., et al. 2018, ApJ, 855, 123
Melosso, M., Melli, A., Puzzarini, C., et al. 2018, A&A, 609, A121
Melosso, M., Belloche, A., Martin-Drumel, M. A., et al. 2020a, A&A, 641, A160
Melosso, M., Melli, A., Spada, L., et al. 2020b, J. Phys. Chem. A, 124, 1372
Motoki, Y., Isobe, F., Ozeki, H., & Kobayashi, K. 2014, A&A, 566, A28
Müller, H. S. P., Schlöder, F., Stutzki, J., & Winnewisser, G. 2005, J. Mol. Struct., 742, 215
Nguyen, T., Fourré, I., Favre, C., et al. 2019, A&A, 628, A15
Ohishi, M., McGonagle, D., Irvine, W. M., Yamamoto, S., & Saito, S. 1994, ApJ, 427, L51
Pickett, H. M. 1991, J. Mol. Spectr., 148, 371
Reid, M. J., Menten, K. M., Brunthaler, A., et al. 2019, ApJ, 885, 131
Remijan, A., Xue, C., Margulès, L., et al. 2022, A&A, 658, A85
Rivilla, V., Martín-Pintado, J., Jiménez-Serra, I., et al. 2019, MNRAS, 483, L114
Rodler, M., Brown, R. D., Godfrey, P. D., & Tack, L. M. 1984, Chem. Phys. Lett., 110, 447
Rodler, M., Brown, R. D., Godfrey, P. D., & Kleibömer, B. 1986, J. Mol. Spectr., 118, 267
Rodríguez-Almeida, L., Rivilla, V., Jiménez-Serra, I., et al. 2021, A&A, 654, L1
Snyder, L. E., & Buhl, D. 1972, ApJ, 177, 619
Theulé, P., Borget, F., Mispelaer, F., et al. 2011, A&A, 534, A64
Turner, B. E. 1991, ApJS, 76, 617
Vinogradoff, V., Rimola, A., Duvernay, F., et al. 2012, Phys. Chem. Chem. Phys., 14, 12309
Zakharenko, O., Motiyenko, R. A., Margulès, L., & Huet, T. R. 2015, J. Mol. Spectr., 317, 41
Zaleski, D. P., Seifert, N. A., Steber, A. L., et al. 2013, ApJ, 765, L10
Zeng, S., Jiménez-Serra, I., Rivilla, V. M., et al. 2018, MNRAS, 478, 2962
Zeng, S., Jiménez-Serra, I., Rivilla, V. M., et al. 2021, ApJ, 920, L27

Table A.1. Harmonic vibrational frequencies of the *E* and *Z* - propanimine determined at the B3LYP/6-311++G(3df,2pd) level of theory and basis set.

Mode	*E* isomer Frequency[a]	*Z* isomer Frequency[a]
1	98.2886	97.9776
2	224.8029	224.9451
3	329.5879	323.7481
4	491.6499	486.0596
5	735.8780	740.2053
6	816.9496	827.4603
7	882.2758	883.8465
8	1017.2856	1012.4935
9	1092.7549	1098.4129
10	1095.3339	1103.6366
11	1127.1635	1140.3170
12	1256.4229	1254.5433
13	1296.3096	1302.0117
14	1337.9349	1343.0188
15	1408.1321	1411.6190
16	1425.2820	1428.3280
17	1478.6041	1477.5019
18	1502.1917	1502.7721
19	1507.4504	1507.1745
20	1718.0731	1715.4981
21	2980.2279	3008.1529
22	3011.0114	3030.2944
23	3027.7075	3037.9972
24	3076.7735	3056.3861
25	3096.6279	3094.8516
26	3100.0702	3100.4317
27	3451.8691	3406.5232

Notes. [(a)]in cm^{-1}.

Appendix A: Vibrational modes of propanimine

Table A.1 provides the harmonic vibrational frequencies of both isomers of propanimine.

Appendix B: Complementary figures: Spectra and population diagram of Sgr B2(N1S)

Figure B.1 shows the transitions of methanimine CH_2NH, v=0 that are covered by the ReMoCA survey and contribute significantly to the signal detected toward Sgr B2(N1S). Figure B.2 shows the population diagram of CH_2NH for Sgr B2(N1S). Figure B.3 illustrates the nondetection of the anti conformer of ethylamine $C_2H_5NH_2$; Figs. B.4 and B.5 the nondetection of vinylamine $C_2H_3NH_3$; Fig. B.6 the nondetection of the Trans-trans conformer of n-propylamine $C_3H_7NH_2$; Fig. B.7 the nondetection of the trans conformer of iso-propylamine i-$C_3H_7NH_2$; Figs. B.8 and B.9 the nondetection of the E and Z isomers of ethanimine CH_3CHNH, respectively; Fig. B.10 the nondetection of ketenimine CH_2CNH; and Figs. B.11 and B.12 the nondetection of the E and Z-propanimine C_2H_5CHNH, respectively. All these figures refer to Sgr B2(N1S).

To compute the LTE synthetic spectrum of the *anti* conformer of ethylamine, we used the CDMS entry (tag 45515, version 1) that is based on the works by Fischer & Botskor (1982) and Apponi et al. (2008). For vinylamine we used the CDMS entries (tags 43504 version 2 and 43508 version 1) that are mainly based on the works by Brown et al. (1990) and Mcnaughton & Robertson (1994). For the *Trans-trans* conformer of *n*-propylamine and the *trans* conformer of *iso*-propylamine we used the spectroscopic work of Melosso et al. (2020b). For the *E* and *Z* isomers of ethanimine we used the spectroscopic work of Melli et al. (2018). For ketenimine we used the CDMS entry (tag 41503 version 2) that is based on the works by Rodler et al. (1984, 1986) and Degli Esposti et al. (2014).

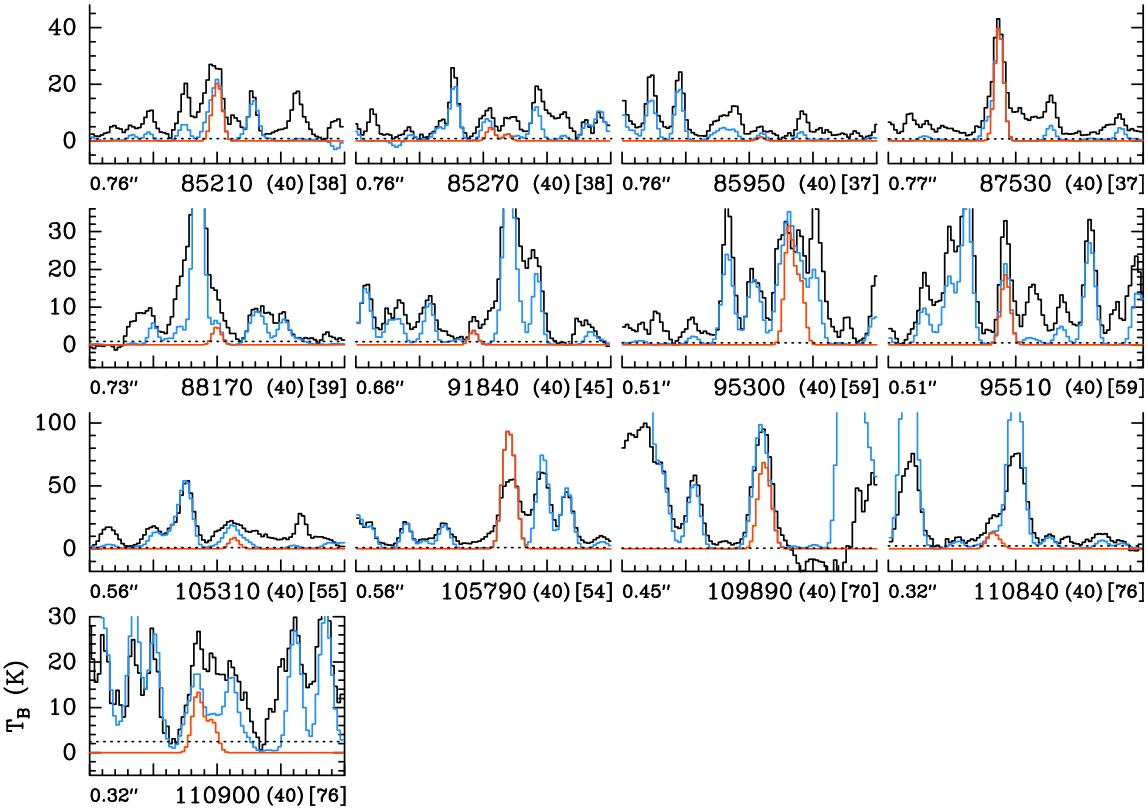

Fig. B.1. Transitions of methanimine CH_2NH, $v = 0$ covered by the ReMoCA survey. The best-fit LTE synthetic spectrum of CH_2NH, $v = 0$ is displayed in red and overlaid on the observed spectrum of Sgr B2(N1S) shown in black. The blue synthetic spectrum contains the contributions of all molecules identified in our survey so far, including the species shown in red. The central frequency is indicated (in MHz) below each panel, the half-power beam width is on the left, the width of each panel (in MHz) is in parentheses, and the continuum level of the baseline-subtracted spectra in K is in brackets. The y-axis is labeled in brightness temperature units (K). The dotted line indicates the 3σ noise level.

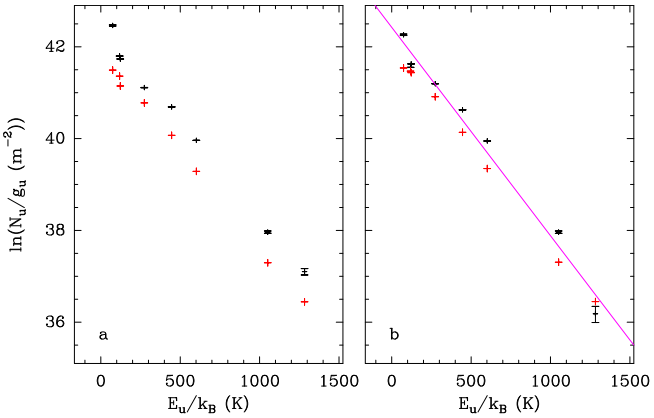

Fig. B.2. Population diagram of methanimine CH_2NH toward Sgr B2(N1S). The observed data points are shown in black, while the synthetic populations are shown in red. No correction is applied in panel **a**. In panel **b** the optical depth correction has been applied to both the observed and synthetic populations and the contamination by all other species included in the full model has been removed from the observed data points. The purple line is a linear fit to the observed populations (in linear-logarithmic space). The rotational temperature derived from this fit is reported in Table 5.

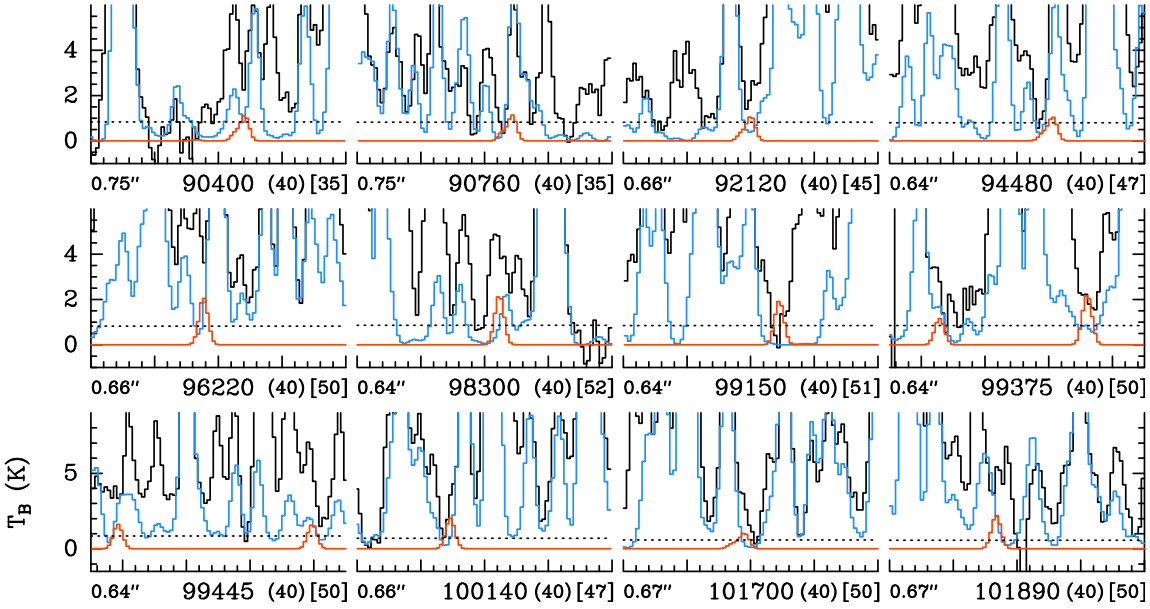

Fig. B.3. Same as Fig. B.1, but the red spectrum shows the synthetic spectrum of ethanamine *anti*-$C_2H_5NH_2$, v=0 used to derive the upper limit on its column density reported in Table 6. The blue spectrum does not contain the contribution of the species shown in red.

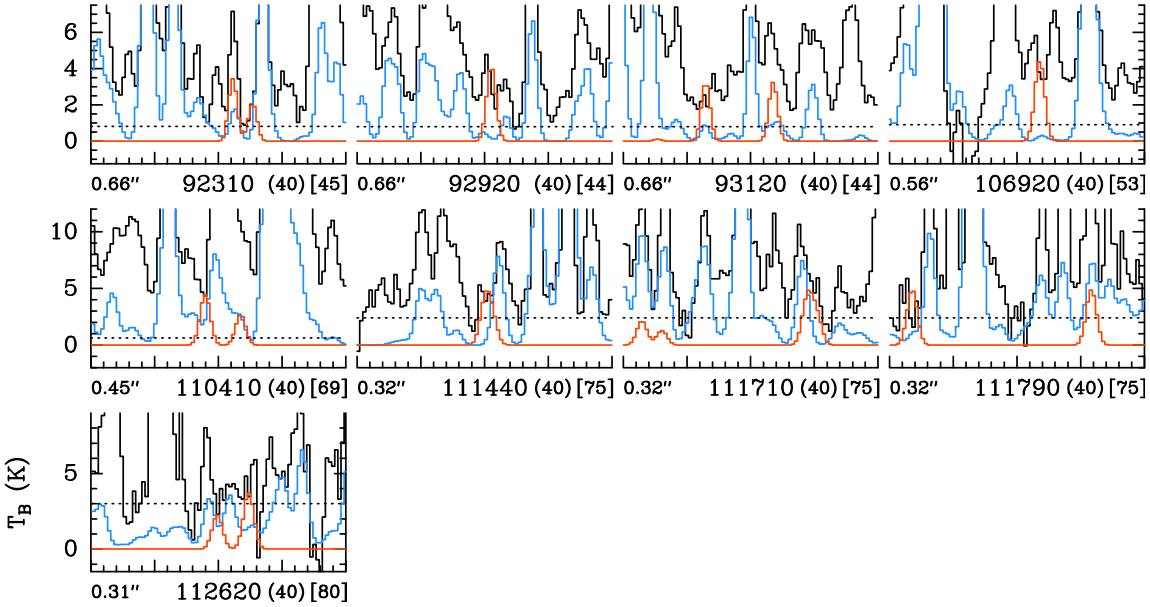

Fig. B.4. Same as Fig. B.3, but for transitions of vinylamine $C_2H_3NH_2$ within the tunneling states 0^+ and 0^-.

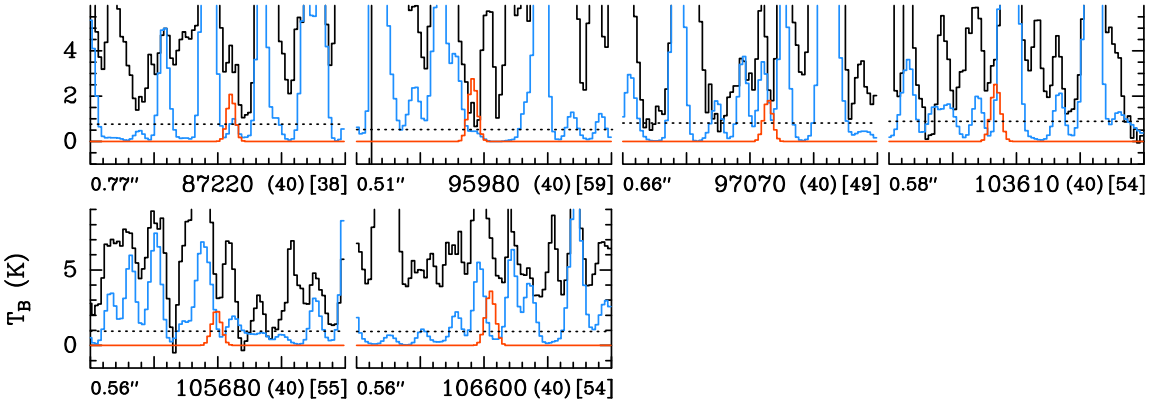

Fig. B.5. Same as Fig. B.3, but for transitions of vinylamine $C_2H_3NH_2$ between the tunneling states 0^- and 0^+.

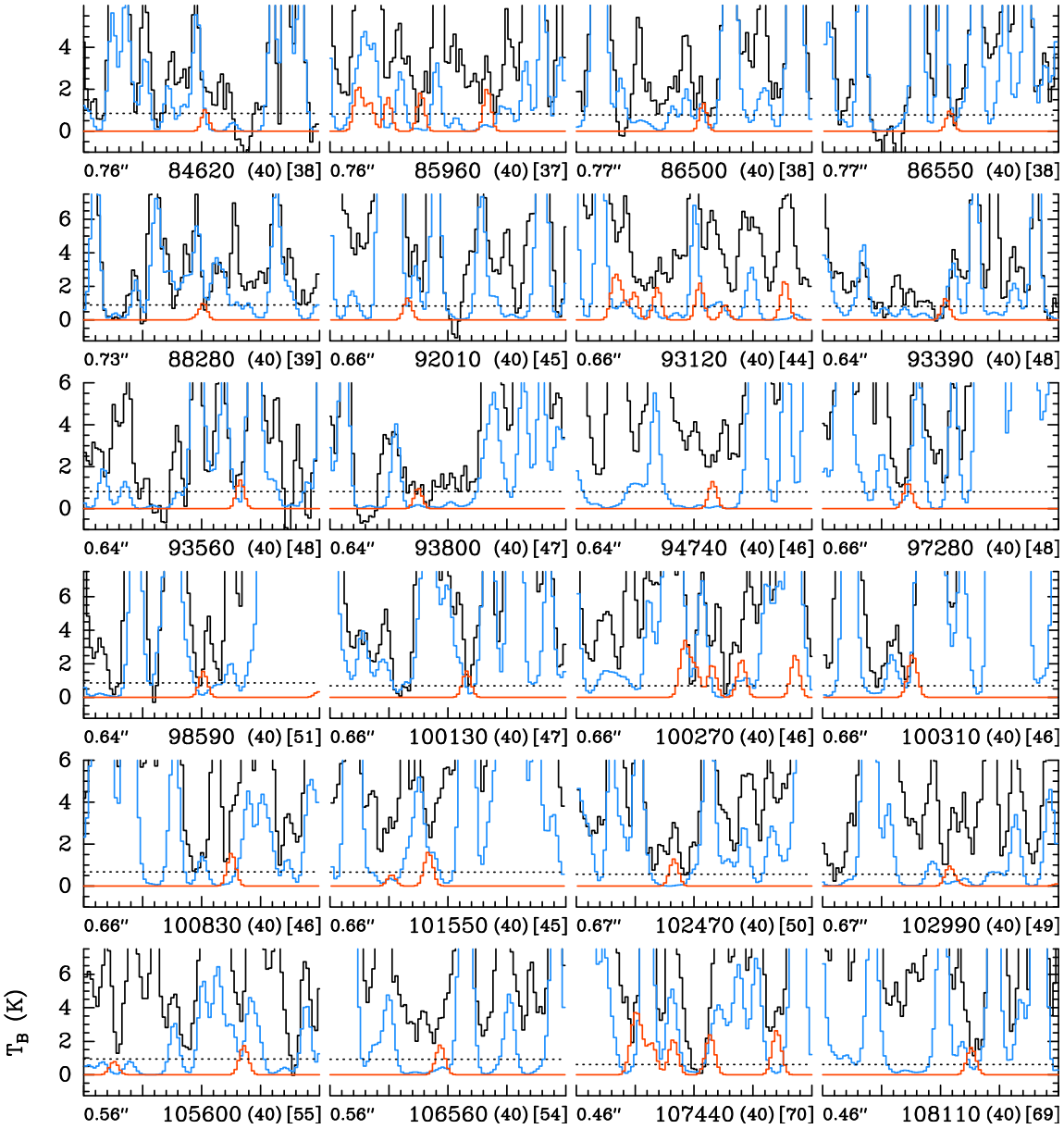

Fig. B.6. Same as Fig. B.3, but for *n*-propylamine *Trans-trans-n*-$C_3H_7NH_2$, v=0.

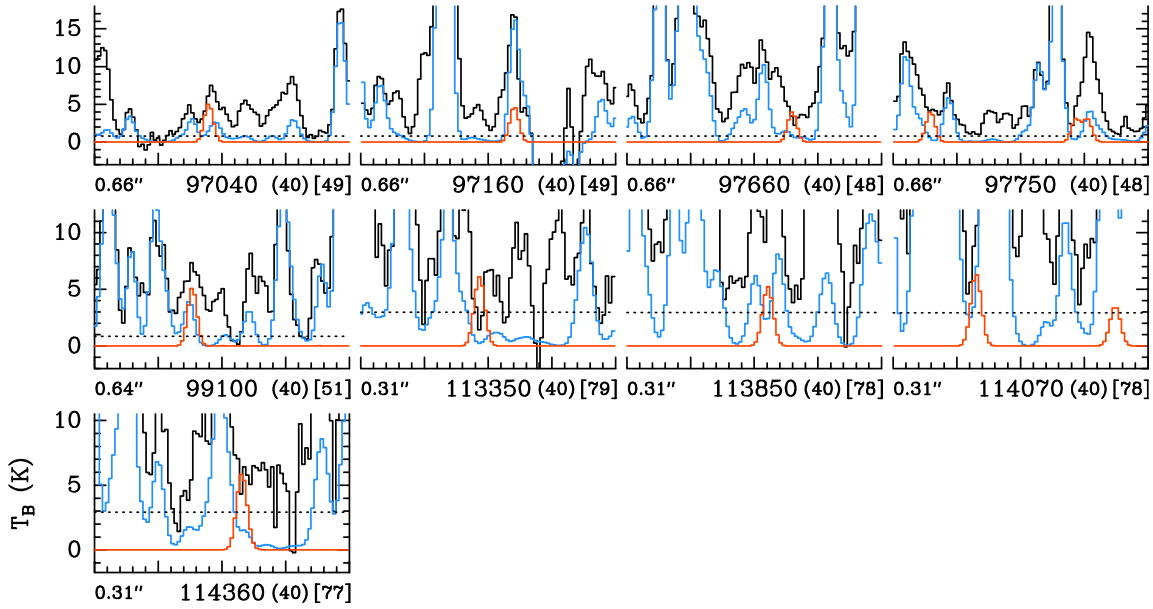

Fig. B.7. Same as Fig. B.3, but for *iso*-propylamine *trans*-*i*-$C_3H_7NH_2$, v=0.

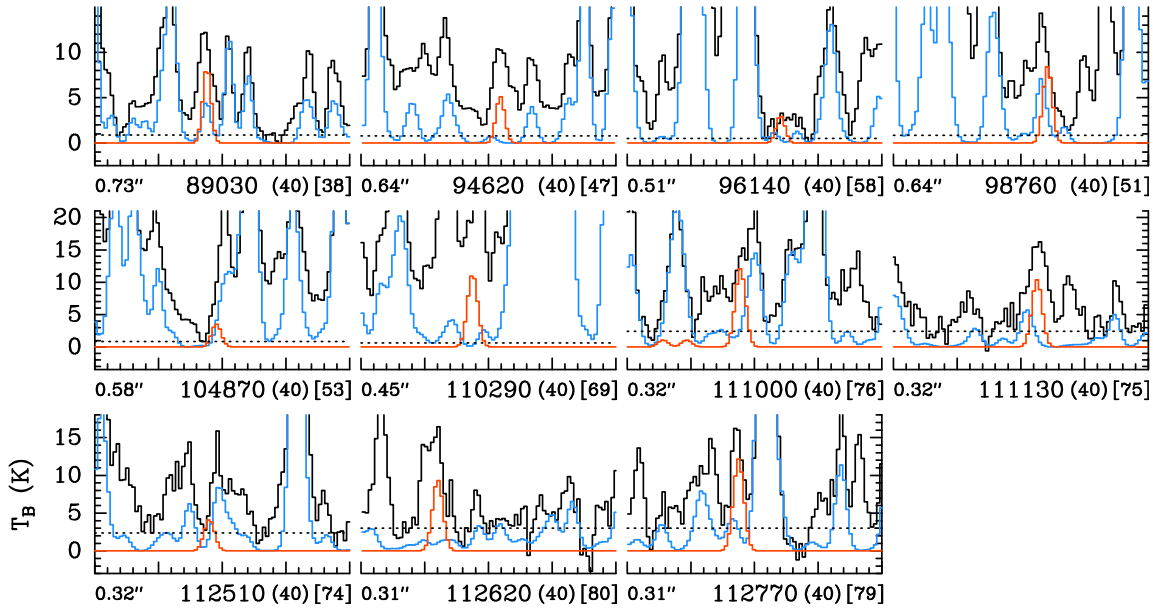

Fig. B.8. Same as Fig. B.3, but for ethanimine *E*-CH_3CHNH, v=0.

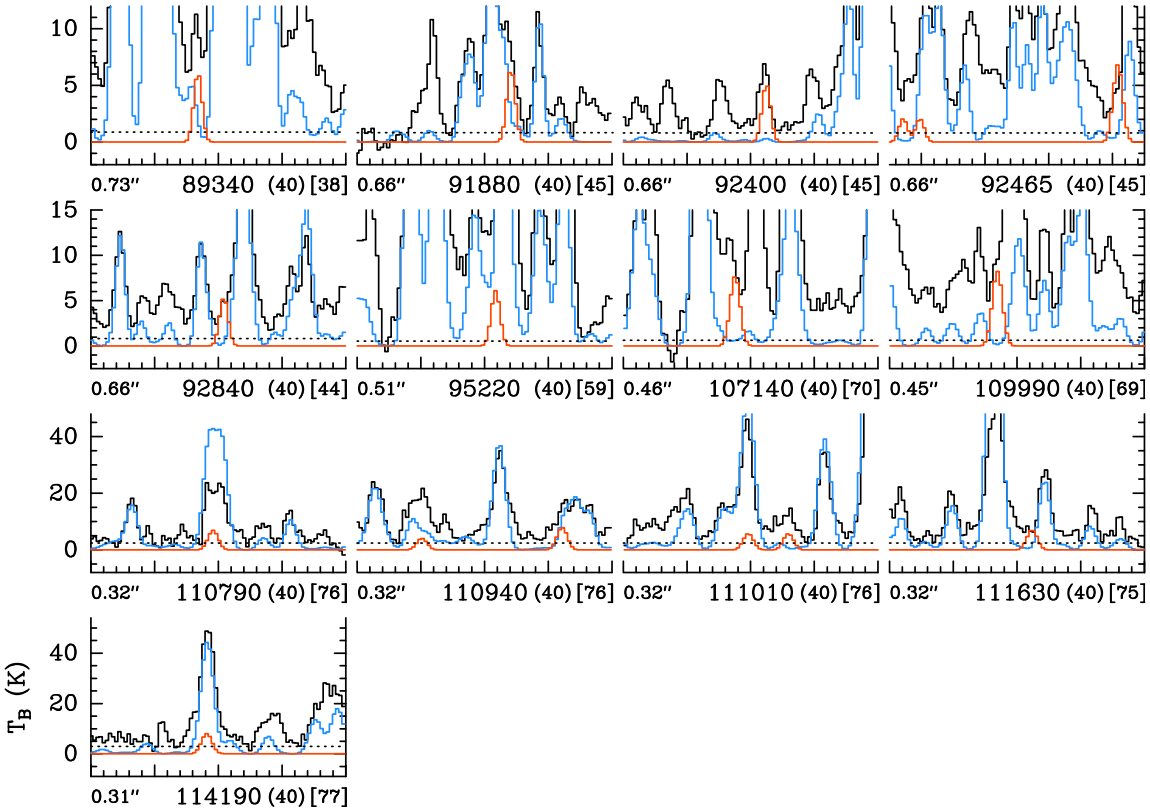

Fig. B.9. Same as Fig. B.3, but for ethanimine *Z*-CH_3CHNH, v=0.

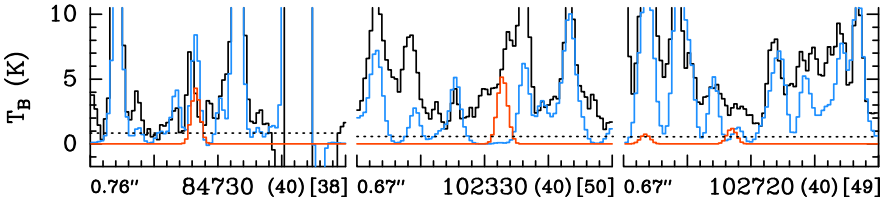

Fig. B.10. Same as Fig. B.3, but for ketenimine CH_2CNH, v=0.

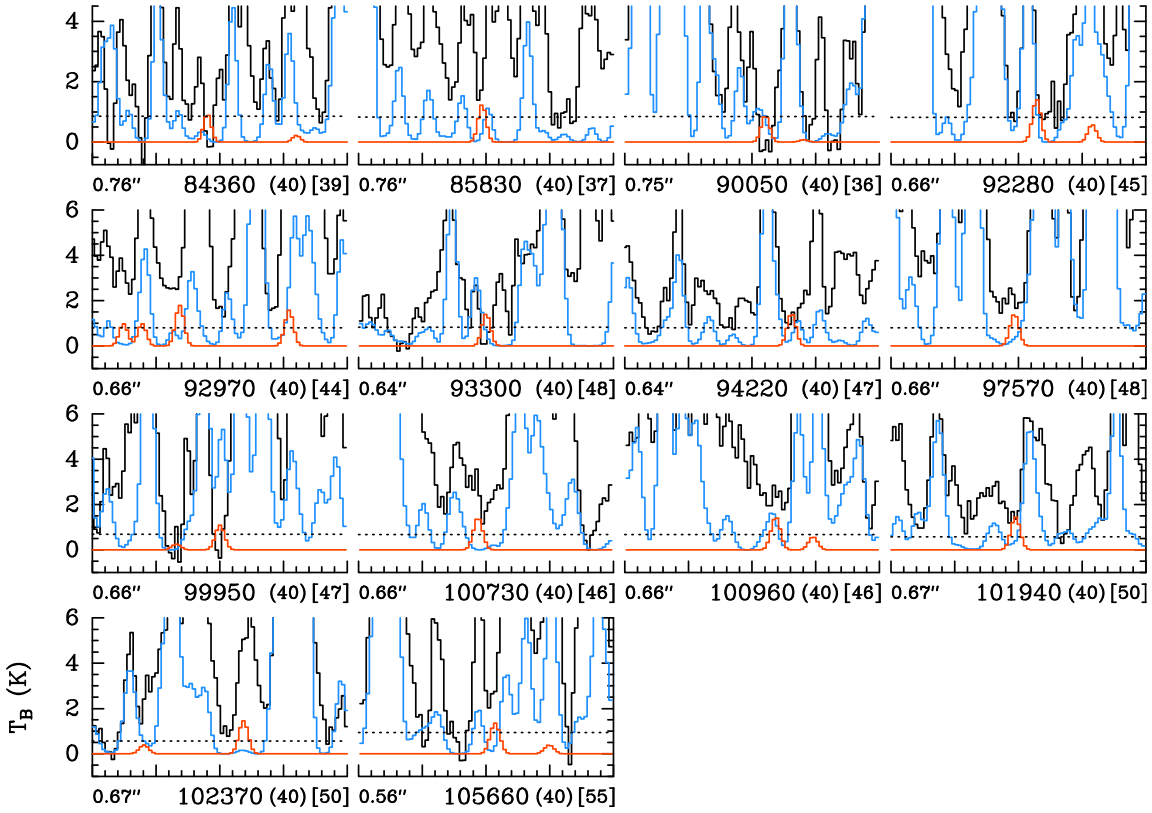

Fig. B.11. Same as Fig. B.3, but for propanimine *E*-C_2H_5CHNH, v=0.

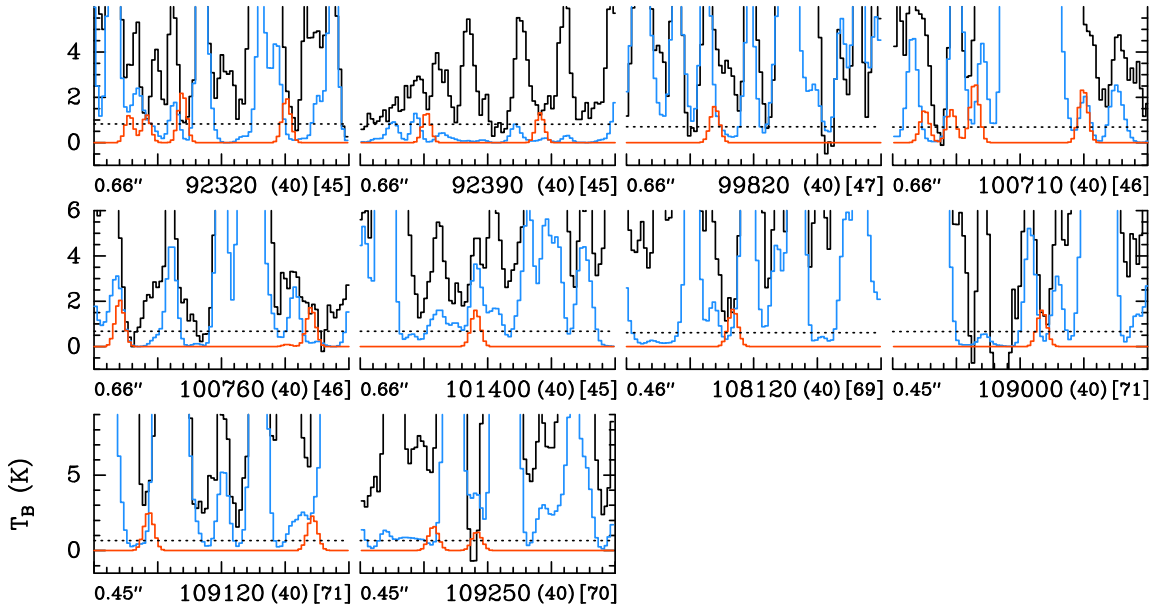

Fig. B.12. Same as Fig. B.3, but for propanimine *Z*-C_2H_5CHNH, v=0.